






Article

GIS-Based Landslide Susceptibility Mapping for Land Use Planning and Risk Assessment

Anna Roccati ¹ , Guido Paliaga ^{1,*} , Fabio Luino ¹ , Francesco Faccini ^{1,2}  and Laura Turconi ¹ 

¹ National Research Council, Research Institute for Geo-Hydrological Protection, Strada delle Cacce 73, 10135 Turin, Italy; anna.roccati@irpi.cnr.it (A.R.); fabio.luino@irpi.cnr.it (F.L.); laura.turconi@irpi.cnr.it (L.T.)
² Department of Earth, Environmental and Life Sciences, University of Genoa, Corso Europa 26, 16132 Genoa, Italy; faccini@unige.it
 * Correspondence: guido.paliaga@irpi.cnr.it

Abstract: Landslide susceptibility mapping is essential for a suitable land use managing and risk assessment. In this work a GIS-based approach has been proposed to map landslide susceptibility in the Portofino promontory, a Mediterranean area that is periodically hit by intense rain events that induce often shallow landslides. Based on over 110 years landslides inventory and experts' judgements, a semi-quantitative analytical hierarchy process (AHP) method has been applied to assess the role of nine landslide conditioning factors, which include both natural and anthropogenic elements. A separated subset of landslide data has been used to validate the map. Our findings reveal that areas where possible future landslides may occur are larger than those identified in the actual official map adopted in land use and risk management. The way the new map has been compiled seems more oriented towards the possible future landslide scenario, rather than weighting with higher importance the existing landslides as in the current model. The paper provides a useful decision support tool to implement risk mitigation strategies and to better apply land use planning. Allowing to modify factors in order to local features, the proposed methodology may be adopted in different conditions or geographical context featured by rainfall induced landslide risk.

Keywords: shallow landslides; analytic hierarchy process (AHP); landslide susceptibility mapping; land planning; risk assessment; Ligurian coast; Mediterranean area



Citation: Roccati, A.; Paliaga, G.; Luino, F.; Faccini, F.; Turconi, L. GIS-Based Landslide Susceptibility Mapping for Land Use Planning and Risk Assessment. *Land* **2021**, *10*, 162. <https://doi.org/10.3390/land10020162>

Academic Editor:

Andrew C Millington

Received: 30 December 2020

Accepted: 27 January 2021

Published: 5 February 2021

Publisher's Note: MDPI stays neutral with regard to jurisdictional claims in published maps and institutional affiliations.



Copyright: © 2021 by the authors. Licensee MDPI, Basel, Switzerland. This article is an open access article distributed under the terms and conditions of the Creative Commons Attribution (CC BY) license (<https://creativecommons.org/licenses/by/4.0/>).

1. Introduction

Landslides are among the most hazardous natural instability processes, which globally lead enormous socio-economical losses and damage to property every year [1–4]. Shallow landslides and debris flows represent one of the major causes of destruction to structures and infrastructures, injured people and casualties in mountain and hilly regions: they are usually triggered by short and severe rainfalls. Shallow landslides generally involve small volumes, unlike debris flows. However, both can be extremely damaging due to their widespread spatial distribution across territories, rapid development and high velocity of propagation [5].

According to Varnes [6], landslide risk can be defined as the probability of the occurrence of a potentially damaging landslide in a given area and for a defined period of time. Hazard assessment requires the estimation of the landslide magnitude, temporal frequency and spatial location [7]. The affectable area and recurrence time are complicated to predict because they are correlated to the complex natural processes that control the mass movement and the difficulty in raising historical landslide data respectively. Surely it could be easier to confine their predictive models to single slopes or very small areas for which detailed physical parameters and historical records can be found. On the other hand, the spatial distribution of potentially unstable areas can be easier to predict by assessing the likelihood of landslide occurrence in a region on the basis of the local ground conditions [8]. Therefore, assessing landslide susceptibility represents the first step in evaluating landslide

risk [9]: identification and mapping of areas where slope instability occurred in the past or with similar physical-mechanical properties are useful to predict the spatial location of future landslide initiation [10].

In this terms, landslide susceptibility assessment and mapping are an essential tool in landslide risk management, supporting authorities, practitioners and decision makers in the more appropriate and sustainable land planning and risk mitigation strategy development, including the implementation of monitoring and warning systems [11–13]. In recent years, several predictive models have been proposed to assess and map the landslide susceptibility, according to the scale and the aims of the analysis, the modelling approaches and the adopted evaluation criteria [7,14,15]. They included both qualitative and quantitative methods. The first type of approach usually returns a landslide susceptibility zonation in terms of weighted indices and relative ranks (e.g., low, medium, high) and are adopted for local scale and site-specific studies; the latter return an estimate of the landslide occurrence as a numerical value. In the recent years, Geographical Information System (GIS) technology has been largely used for landslide susceptibility assessing and mapping, frequently combined with data detected by innovative techniques, e.g., satellite remote sensing and light detection and ranging (LiDAR) images. GIS-based models allow to manage big volumes of data, both in terms of file size and geographical scale, and to perform a dynamic and on-going landslide susceptibility zonation, which represents an essential requirement for a proper land-planning and risk mitigation [16–19].

According to several authors [7,15,20,21] methods proposed to assess landslide susceptibility can be classified into (i) qualitative geomorphological mapping and analysis of landslide inventories, which depend on the ability and experience of the researcher and the quality and completeness of the catalogues respectively [22–24]; (ii) semi-quantitative heuristic or index-based approaches, which rely on the level of understanding of the geomorphological processes and the correlation between predisposing and triggering landslide causal factors in order to rank and weight features responsible for instability, according to their importance, expected or assumed, in triggering landslides [25–27]; (iii) physically based methods, relying on the understanding of the physical laws which control the slope stability, usually adopting a simple limit equilibrium model, e.g., infinite slope stability model, or more complex ones [28–30]; (iv) statistical methods, based on the analysis of the functional correlations between instability factors and the past/present landslide spatial distribution, e.g., bivariate or multivariate analysis, linear and logistic regression, artificial neural network, fuzzy logic, etc. [31–33].

Among heuristic approaches, the analytic hierarchy process (AHP) method has been largely applied in literature for landslide susceptibility analysis [34–37]. AHP belongs to the multicriteria techniques, which are largely applied in natural hazard management [38] thanks to their capability in relating heterogeneous physical quantities [39]. Through a matrix-based pair-wise comparison, this multiple criterion decision-making tool enables one to analyze and compare the contribution of the different environmental factors involved in landslide occurrence, which usually present a spatial and temporal variability.

In this paper, the semi-quantitative AHP method has been adopted to compute the landslide susceptibility of the Portofino promontory, Northern Italy, which represents a hilly mountain Mediterranean coastal area famous in the world for its great natural and cultural landscapes, historically affected by shallow landslides and debris flows. Starting from the catalogue of past landslides, nine natural and anthropic conditioning factors have been selected, and different weight coefficients have been assigned to each of them and each associated class adopting the AHP approach. Then, the weighted variables have been combined and ranked into five different susceptibility levels. Finally, the resulting landslide susceptibility map has been compared to the landslide susceptibility zonation which is currently used by stakeholders in the regional and municipal land-planning and risk management. Our study aims to highlight the difference between the two susceptibility models and how a recurrent spatial analysis of landslide distribution at local scale is essential to update the knowledge of the areas where shallow landslides and debris flows

may occur in the future, so that the most effective land management and successful prevention of landslide risk can be provided. Further, including anthropogenic factors in conditioning corresponds to the added effects of human activity on the Earth's surface, which considers man as a morphogenetic factor. The effects of human modification, that may assume a very high importance locally, may result even in landslide generation. In this sense the diffuse presence of abandoned man-made terraces may result in a possible source of shallow landslides.

2. Materials and Methods

2.1. Study Area

The Portofino Promontory extends for 23 km² in the eastern Liguria, Northern Italy, between Genoa Gulf (W) and Tigullio Gulf (E) (Figure 1). It is world-famous for the attractive landscapes and seascapes and its natural, historical and cultural heritage. Well-known settlements of great value and seaside resorts stand along its coast, such as Camogli, San Fruttuoso, Portofino, Paraggi and Santa Margherita Ligure. Because of the great environmental and cultural values, the promontory is protected and included in the Regional Natural Park of Portofino (18 km²) since 1935, including the seaward area that became a marine reserve in 2001, when the boundaries of the protected area have been redefined.

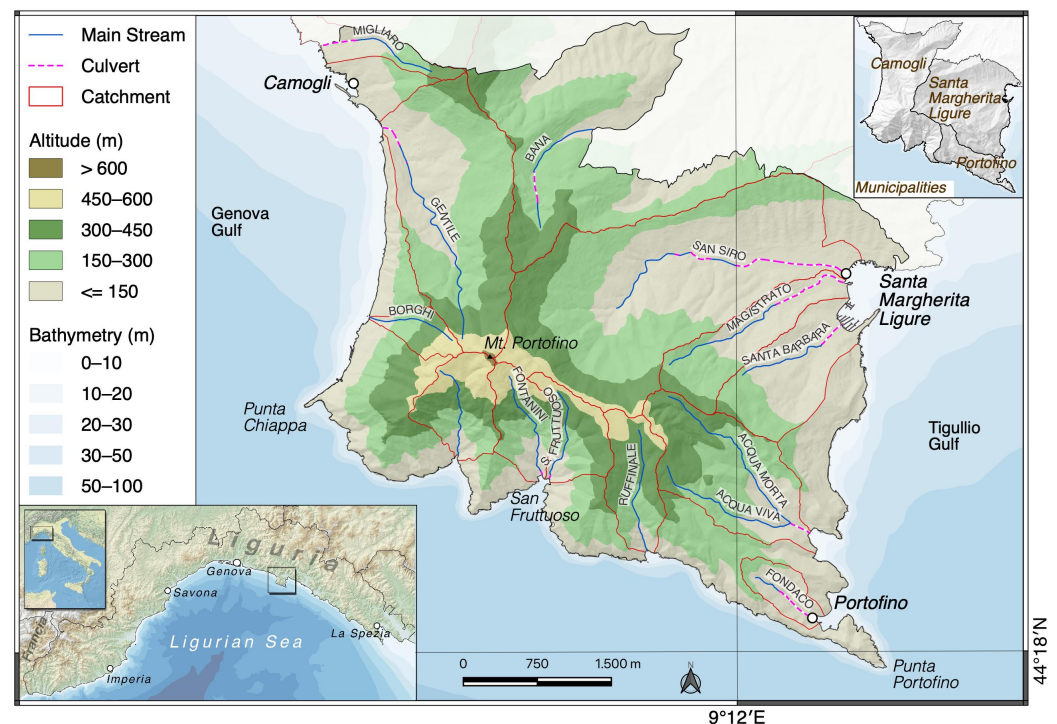


Figure 1. Location of the study area and geographical setting of the Portofino promontory.

The geological setting of the promontory is made by a sedimentary rock masses, with conglomerate and flysch [40,41]. The Conglomerate of Portofino (Oligocene) crops out in the southern sector, particularly along the steep slopes and high cliffs between Punta Chiappa and Portofino, and secondarily along the south-eastern coastal stretches, between Portofino and Punta Cervara. Conglomerate is made up of heterogeneous clastic elements, mainly of marly limestone, sandstone, limestone and secondarily of other lithotypes, in a sandy-limestone matrix. The formation features a fragile deformation tectonic, with several fault and fracture systems oriented mainly NW-SE and NE-SW, both at the meso- and macro-scale [42]. The Flysch of Mt. Antola (Cretaceous Sup. – Paleocene) is made up of marly limestone layers ranging in thickness from decimeters to meters, with shales, siltstones and calcarenites interlayers. It forms the central and norther sectors of the

promontory and widely crops out along the western slopes between Scogli Grossi and Castellaro. The formation has been involved in a complex polyphase deformation tectonic, both ductile and fragile, with large-scale folds with SSW vergence and WNW-ESE axis orientation [43,44] which are well exposed along the cliffs.

Several fracture and direct fault systems, with different directions, control both geological and morphological settings of the promontory. The drainage pattern and the coastline and ridge orientation are the result of the extensive tectonic activity that affected the Ligurian continental margin during the Quaternary [45,46].

The peculiar geological and morphological setting is responsible for the widespread instability processes, which affected large portions of the promontory, locally caused by erosional processes and undercutting produced by running water and sea wave action along slopes and cliffs. Most of the mass movements developed along the contact between the formations, due to the different geomechanics behavior: the two largest landslides are quite close to the tectonic contact, at Le Gave (eastern sector) and San Rocco (western sector) [47–49] (Figure 2A,B). Rockfalls and shallow landslides, including rapid and destructive mud and debris flows, are involved frequently in the southern steep sectors shaped in the conglomerate, whereas landslides characterized by different movement types, including sliding and complex landslides, affected the gentler slopes shaped in the marly limestone flysch [50,51] (Figure 2C,D). Recurrent falls and topples occurred along the high cliffs made up of both conglomerate and flysch, also favored by the sea wave action generally triggered by SW (*Libeccio*, dominant) and SE (*Scirocco*, prevailing) winds depending on the orographic orientation (Figure 2E,F).

Mountains with high elevations (up to 600 m a.s.l.) close up the coastline and high cliffs (up to 200 m) characterize the southern and western sectors: slopes face mainly from SE to W, with high to very high steepness values ranging from 50% to 75%, which locally exceed 75% along the cliffs. Whereas the eastern and northern sectors of the promontory are featured by gentle hills, with prevalently E- and NE- facing slopes and steepness values ranging generally from 10% to 50%. A very small coastal floodplain (<0.5 km²) occupies the final stretch of San Siro, Magistrato and Santa Barbara Creeks, where the town of Santa Margherita Ligure stands (Figure 1).

Catchments have a high slope gradient, and they are generally small to very small in size (less than 1 km²), except for few of them which extend up to 5 km² (Acqua Morta and San Siro creek, Gentile stream and the upper Boate stream basin). Consequently, their hydrologic response to rainfall events is quite rapid, with time of concentration typically less than 1–2 h. Watercourses are generally short, steep and incised, with a typical angular pattern, as a result of the high relief and tectonics control. Streams are frequently dry, particularly in summer months or during prolonged dry spell; however, during heavy rainfall events, they can reach more considerable discharges with a large solid transport, thereby evolving into rapid mud or debris flows.

Forests (950 ha) and shrub and/or herbaceous vegetation association (200 ha) occupy large sectors of the promontory. Forested areas include broad-leaved forests (640 ha), coniferous forest (124 ha) and mixed forest (186 ha). High cliffs and the steep S-facing slopes have little or no vegetation (75 ha), followed by sparse vegetation (58 ha), bare rocks (15 ha), whereas small pebbly beaches are in the little bays (<2 ha). The northern and eastern hilly sectors are largely occupied by permanent crops (667 ha), including olive groves (665 ha) and vineyards (<2 ha), heterogeneous agricultural areas (21 ha), pastures (2 ha) and arable lands (<1 ha). Terraces characterize large sectors of the Portofino promontory, totally modifying the former natural landscape: they are widespread both in the current agricultural lands, largely represented by olive groves, in use or abandoned, and in re-vegetated areas or in totally abandoned ones [51]. Artificial areas represent a very small portion of the territory: urban fabric (247 ha), industrial, commercial and transport units (32 ha) and artificial, non-agricultural vegetated areas (33 ha) occupy small stretched of the coastal slopes and floodplain.

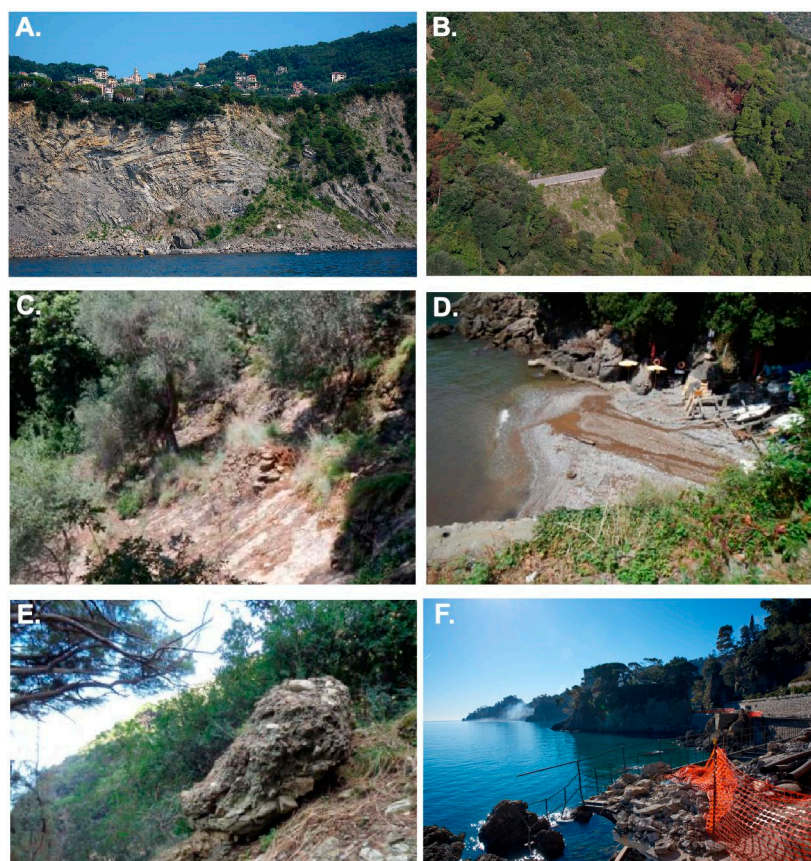


Figure 2. (A) Panoramic view of the western slope of the Portofino promontory below San Rocco village historically affected by mud-debris flows, shallow landslides and rock falls (photo G. Stagni). (B) A recent view of the relict coastal landslide at Le Gave from above, on the eastern slope. (C) Source area of the mud-debris flows triggered on 26 July 2014, generated by the collapse of some terraces. (D) Mud and debris at the outlet of the San Fruttuoso creek resulting from the collapse of some terraces upstream due to intense rainfall event on 26 July 2014, which caused damage to some tourist facilities in the historical village. (E) Rock fall involved conglomerate outcropping bedrock at San Fruttuoso on 25 October 2016. (F) Damage on the road along the coastline between Santa Margherita and Portofino on 27–28 October 2018, caused by a sea storm surge.

The complex geological, climate and environmental history and setting contribute also to a significant spatial pedological variability in the soil horizons of the Portofino promontory with six different Reference Soil Groups [52] and evidence of an extensive ancient erosional surface and several paleosol features, suggesting the existence of different tectonic and climate conditions that have been responsible for erosion phenomena [53].

The climate of the Portofino promontory is conditioned by the local orographic configuration: the presence of a mountain relief which exceed 600 m close to the sea (<1 km) and the slopes aspects, determine peculiar insolation and exposure conditions to marine winds, with a significant spatial climate variability. The climate is Mediterranean, with hot and dry summers and mild winters in the southern, and changeable, rainy weather; whereas a mid-hill zone, with more abundant precipitations and colder winters, characterizes the northern sectors. Regime rainfall ranges depending on the orographic setting, with maximum rainfall in autumn, and minimum rainfall in summer [54]. Intense and short duration rainfalls frequently occur in late summer or autumn months, from August to November, generated by a typical atmospheric circulation over the Genoa Gulf, called Genoa Low [55,56] usually associated with intense thunderstorms [57]: the resulting convective systems generate localized and severe precipitation, which are frequently responsible for flash floods and widespread shallow landslides and mud-debris flows [51,58,59].

2.2. Data and Research Methodology

A catalogue of rainfall-induced rapid and very rapid mass movements occurring in the study area since 1910 has been compiled. In particular, gravitational processes with high to very high velocity of the movement of variable volumes of materials triggered by rainfall events, including shallow landslides, mud or debris flows and rock falls, were considered. Information was gathered from different sources, including scientific papers, technical reports, archives of local municipalities and newspaper articles [59]. Most of the historical data derive from the inventory of sites historically affected by landslides and floods events in Italy in the period 1918–1994 of the AVI Project (Hit Areas of Italy) of GNDICI-CNR (National Group for Geo-hydrological Disaster Protection of National Research Council) [60].

Using regional base maps at 1:10,000 scale (Table 1), landslides have been georeferenced within a GIS Geographical Information System open source software (QGIS 3.10). Since areal information on landslide size has been difficult to retrieve due to the heterogeneous source types, punctual features have been adopted, which represents the highest point of the landslide scarp. Simultaneously, for each landslide feature the following information has been recorded [59]: (i) landslide type [5,61]; (ii) geographical location and its spatial accuracy, from P1 (approximate location of slope failure within a buffer area < 1 km²) to P3 (buffer area > 10 km²); (iii) data of the landslide occurrence; (iv) source of landslide information and/or archive where bibliographic research was carried out.

In addition to the past rainfall-induced landslides inventory, the set of thematic maps listed in Table 1 has been used to analyze the correlation between slope failures and both natural and anthropic predisposing factors, and to generate the landslides susceptibility map of the study area.

Table 1. Vector (V) and raster (R) data used. CTR, Regional Topographical Cartography; CORINE, Coordination of Information on the Environment [62]; DTM, Digital Terrain Model; IFFI, Italian Landslide Inventory [63].

Name	Source	Scala/Pixel	Date	Type
Administrative Unit	Liguria Region	1:5000	2018	V
Aspect	Liguria Region	1:10,000	2007	V
Buildings, Manufacts and Walls (CTR, 2nd Ed. 3D)	Liguria Region	1:5000	2007	V
CORINE Land Use (II Level)	Liguria Region	1:10,000	2018–2019	V
CTR	Liguria Region	1:5000	1990–2006	R
DEM	Liguria Region	5 m	2016	R
Hydrographic Network and Catchments	Liguria Region	1:10,000	2019	V
Landslide, Project IFFI	Liguria Region	1:10,000	2014	V
Lithology	Liguria Region	1:10,000	2017	V
Nature Reserve Borders	Liguria Region	1:10,000	2019	V
Orthophotography	Liguria Region	0.15 m	2004	R
Orthophotography	Google Earth	2.5 m	2019	R
Pedological Map	Rellini et al. [53]	1:10,000	2017	R
Road network, CTR 2nd Ed. 3D	Liguria Region	1:5000	2007	V
Slope	Liguria Region	1:10,000	2016	V
Springs	Faccini et al. [64]	1:10,000	2018	V
Terraced areas	Paliaga et al. [51]	1:5000	2020	V
Trail Network	Liguria Region	1:25,000	2020	V

2.3. Landslide Conditioning Factors

Rainfall is commonly recognized as the major landslide causative elements [65]: shallow landslides and mud-debris flows triggered by very short, but intense or prolonged, rainfalls can be particularly destructive due to their spatial distribution and rapid propagation. However, several natural factors control the slope stability, including lithology,

topography, hydrographical network, land use and geomorphological processes can affect the initiation of slope failures. Several researches highlighted the relationship between shallow landslides occurrence and human activities [66–69]: deforestation for farming, modifications in drainage patterns and slope profile due to artificial road cuts, fills or other construction purposes, reduce the rainfall infiltration and increase the erosional processes by surface run-off, predisposing slope to collapse.

In order to assess the landslide zonation of the Portofino promontory, the spatial relationships among the rainfall-induced rapid mass movements that occurred in the study area from 1910 to 2019 have been analyzed, and natural and anthropic landslide conditioning factors have been selected. In particular, the following nine thematic variables have been selected: (i) lithology, (ii) slope aspect, (iii) slope acclivity, (iv) land use, (v) terraced landscape, (vi) hydrographic elements distance, (vii) distance to man-made cuts elements, (viii) distance to man-made structures and (ix) existing gravitational processes (Table 2).

Table 2. Landslide conditioning factors and correlated classes used in the analysis.

Conditioning Factor	Number of Classes	Classes
Lithology	5	Heterogeneous clayey and sandy materials (<i>Alluvial deposits</i>)
		Incoherent soils (<i>Thick slope covers</i>)
		Heterogeneous materials of anthropic origin (<i>Fills and artificial deposits</i>)
		Marly limestone and marls (<i>Flysch of Monte Antola</i>) Conglomerate (<i>Conglomerate of Portofino</i>)
Aspect	9	North
		North-east
		East
		South-east
		South
		South-west
		West
		North-west Zenith
Acclivity	7	0–10%
		11–20%
		21–35%
		36–50%
		51–75%
		76–100%
		>100%
Land use	10	Urban fabric
		Industrial, commercial and transport areas
		Artificial, non-agricultural areas
		Arable land
		Permanent crops
		Pastures
		Heterogeneous agricultural areas
		Forests
		Shrubs and/or herbaceous vegetation association Open spaces with little or no vegetation
Terraced area	2	Presence of terraces
Hydrographic elements	4	Spring, distance < 10 m
		Watercourses, distance < 10 m
		Spring, distance > 10 m
		Watercourses, distance > 10 m

Table 2. *Cont.*

Conditioning Factor	Number of Classes	Classes
Man-made cuts	4	Trial, distance < 5 m
		Main road, distance < 5 m
		Minor road, distance < 5 m
		Man-made cuts, distance > 5 m
Man-made structures	4	Buildings, distance < 10 m
		Other manufacts, distance < 10 m
		Retaining walls, distance < 10 m
		Man-made structures, distance > 10 m
Existing Landslide (IFFI)	6	Active/reactivated/suspended
		Dormant
		Inactive/stabilized
		Area affected by widespread shallow landslides
		Assumed stable area, distance < 50 m
		Assumed stable area, distance > 50 m

2.3.1. Lithology

It is generally known that geological and structural settings can affect the initiation and development of shallow landslides [70,71]. We considered five classes derived from the thematic regional map at 1:10,000 scale (Table 1) and based on the lithological features (Figure 3A): (i) heterogeneous clayey and sandy materials, which form the alluvial deposits; (ii) incoherent soils, including silt and clay with granular fraction and coarse soils, which form the thick slope covers; (iii) heterogeneous materials of anthropic origin, which include fills and artificial deposits; (iv) marly limestone and marls (Flysch of Monte Antola) and (v) conglomerate (Conglomerate of Portofino), with eluvial and colluvial deposits.

2.3.2. Slope Aspect

Among morphological factors, aspect plays a relevant role in slope stability, inducing different conditions of insolation, temperature, land cover, weather conditions and rainfall exposure and, therefore, controlling important properties of the soils, e.g., temperature, moisture and level of saturation [28,72]. Landslide occurrence is more common on south-facing slopes than on north slopes, where failures occasionally occur due to the presence of more vegetation covers that can increase soil strength and reduce water infiltration [73,74]. Adopting the regional thematic map at 1:10,000 scale (Table 1), we considered the nine aspect classes shown in Figure 3B.

2.3.3. Slope Acclivity

Acclivity plays also a relevant role in the activation of instability processes [75,76]. We derived the topographical information from the regional technical map at 1:10,000 scale (Table 1), where slope steepness (in percentage) has been organized in seven classes, from 0 to 10% to >100% (Figure 3C).

2.3.4. Land Use

Several studies highlighted the relevant role of land use and changes in land use in triggering shallow landslide [67,77], in addition to the other geological and morphometric predisposing factors. We used the regional land use map at 1:10,000 scale based on the CORINE nomenclature [62]. In particular, we considered ten land use categories of second level (Figure 3D): (i) urban fabric, (ii) industrial, commercial and transport areas, (iii) artificial, non-agricultural areas, (iv) arable land, (v) permanent crops, (vi) pastures, (vii) heterogeneous agricultural areas, (viii) forests, (ix) shrubs and/or herbaceous vegetation association and (x) open spaces with little or no vegetation, including beaches and bare rocks.

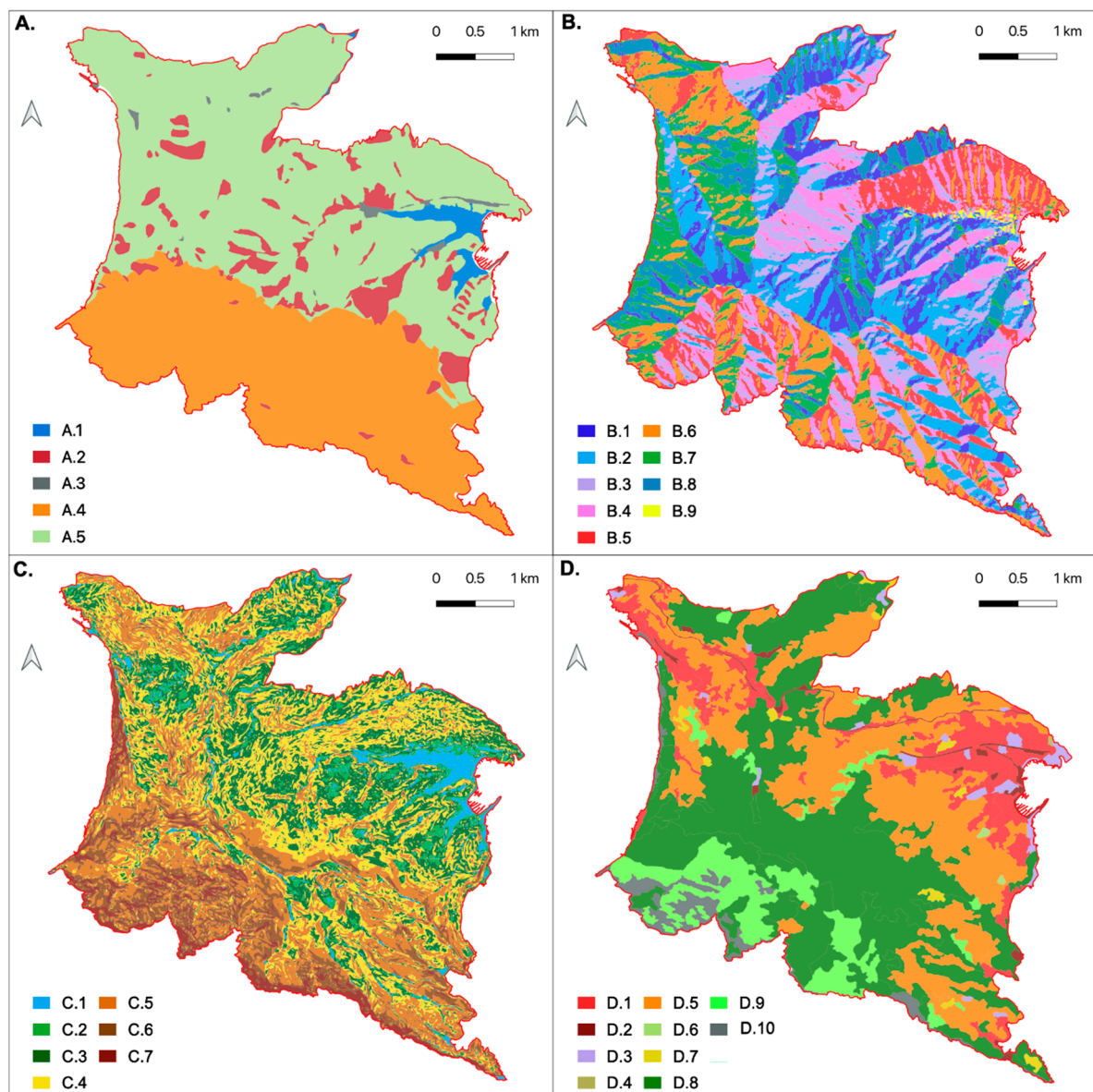


Figure 3. Shallow landslides predisposing factors. **(A)** Lithology: 1. Heterogeneous clayey and sandy materials (Alluvial deposits); 2. Incoherent soils, including silt and clay with granular fraction and coarse soils (Slope deposits); 3. Heterogeneous materials of anthropic origin (Fills and artificial deposits); 4. *Marly limestone and marls* (Flysch of Monte Antola); 5. Conglomerate (Conglomerate of Portofino). **(B)** Slope aspect: 1. North; 2. North-East; 3. East; 4. South-East; 5. South; 6. South-West; 7. West; 8. North-West; 9. Zenith. **(C)** Slope steepness: 1. 0–10%; 2. 11–20%; 3. 21–35%; 4. 36–50%; 5. 51–75%; 6. 76–100%; 7. >101%. **(D)** Land use, based on the 2° level of CORINE nomenclature (European Environmental Agency, 1995): 1. Urban fabric; 2. Industrial, commercial and transport units; 3. Artificial, non-agricultural areas; 4. Arable land; 5. Permanent crops; 6. Pastures; 7. Heterogeneous agricultural areas; 8. Forests; 9. Shrubs and/or herbaceous vegetation association; 10. Open spaces with little or no vegetation.

2.3.5. Terraced Landscape

Several studies have investigated the role of terraced landscapes in slope stability. One hand, cultivated terraces control runoff processes on steep slopes, erosion and rainfall infiltration, reducing the geo-hydrological risk; as a consequence, progressive terrace abandonment may affect negatively the stability of the slope in response to very intense rainfall events [78–81]. On the other hand, recent studies highlighted how the growth of natural vegetation on abandoned terraces increases the slope stabilization and, at the

same time, how rainfall-induced shallow landslides affected both vegetated abandoned and well-maintained cultivated terraces [51,82,83]. Unlike authors who did not compute terraces in landslide susceptibility estimation [36], we included terraced landscape among the anthropic variables that may influence the shallow landslides initiation. Terraced surfaces in the study area are shown in Figure 4A: they have been detected carrying out the semi-automatic technique [51] for the terrace identification in the portion of Portofino promontory within the Natural Park boundaries, using the raster data listed in Table 1.

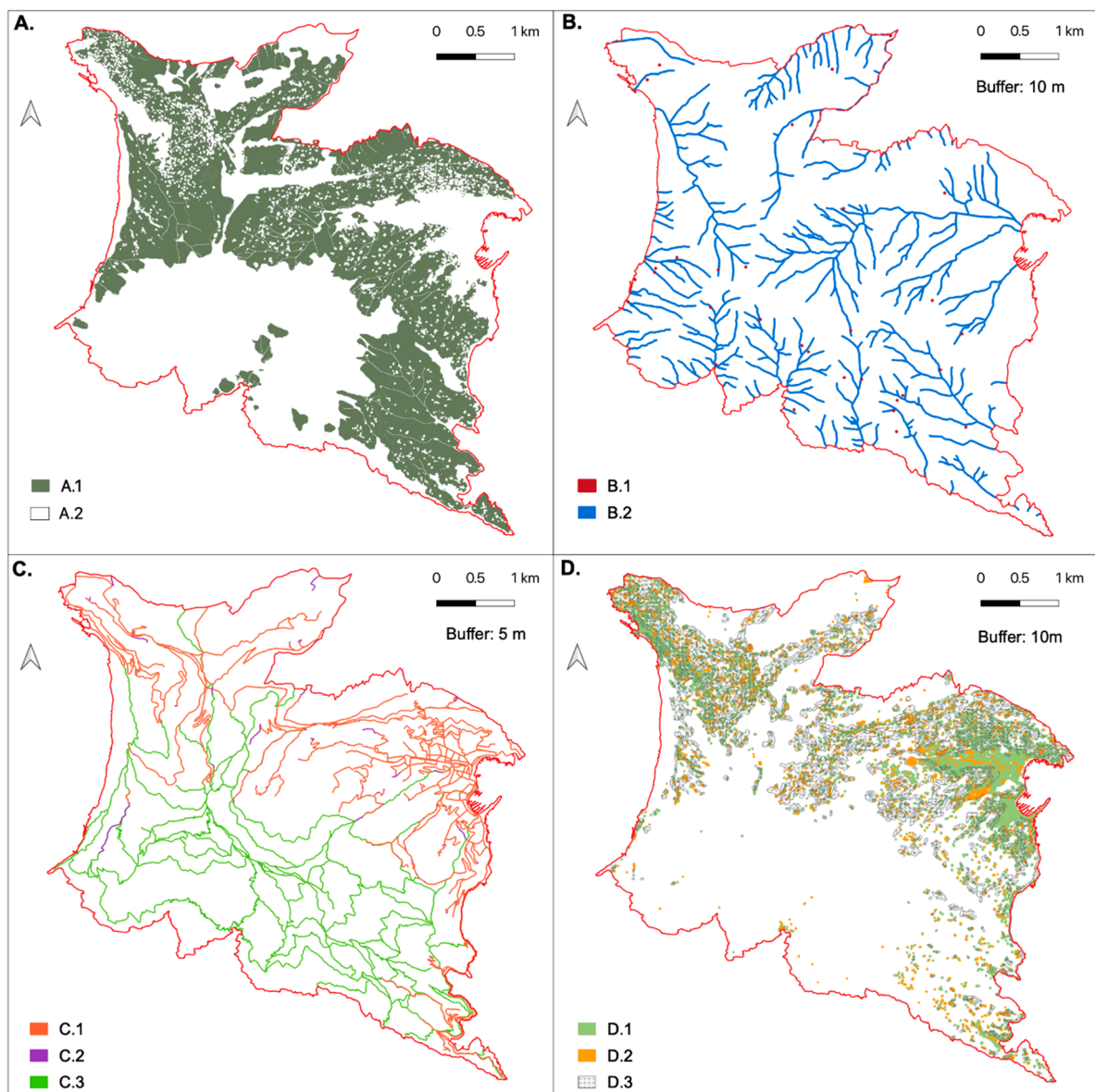


Figure 4. Shallow landslides predisposing factors. (A) Terraces: 1. Terraced area; 2. Non-terraced area. (B) Distance from hydrographic network (buffer zone = 10 m): 1. Springs; 2. Watercourses. (C) Man-made cuts (buffer zone = 5 m): 1. Main road network; 2. Minor road network; 3. Trail network. (D) Man-made structures (buffer zone = 10 m): 1. Buildings; 2. Other manufactures; 3. Retaining walls.

2.3.6. Hydrographic Elements Distance

Proximity to hydrographic networks, including watercourses and springs, may affect the slope stability [33,34,84]. Morphological modifications due to gully erosion may influence the removal of incoherent materials and the activation of mass movements, particularly along steep slopes [85]; furthermore, watercourses may affect the slope stability

by saturating the lower part of geomaterial and increasing the water level, particularly in cases of permeable bedrock due to lithological or mechanical properties. We derived water-courses and springs in the Portofino promontory from the regional thematic map at 1:10,000 scale (Table 1). To analyze their effects on shallow landslides triggering, we produced a buffer map where streams and springs are buffered at distance of 10 m (Figure 4B).

2.3.7. Man-Made Cuts and Structures Distance

Similarly, anthropogenic changes to slope profile and runoff network induced by cut-and-fill works can modify the stress-strain and drainage conditions, modifying the slope equilibrium and increasing the possibility of shallow landslides activation [86–88]. Slope cuts, such as roads or trails segments, frequently represent the source of failure [33,89,90]; but they can also act as a barrier or a preferential flow-path route, cutting the natural drainage network. The influence of road and trail networks distance on shallow landslide was analyzed, setting a buffer zone of 5 m around the linear elements (Figure 4C). In particular, we considered both main and minor road features, extracted from the regional topographical database, and the trail network of the Portofino promontory derived from the correlate regional technical map (Table 1).

To analyze the influence of man-made structures distance on landslide occurrence, we extracted buildings, manufacts and retaining walls from the regional topographical database (Table 1) and buffered the features at a distance of 10 m (Figure 4D).

2.3.8. Existing Gravitational Processes

We also considered the presence of pre-existing landslides, which may represent areas with a potential higher proneness to slope instability. These instability processes derived from the regional catalogue of landslides at 1:10,000 scale [63] (Table 1), in which landslides are mapped and classified on the basis of type of movement and state of activity. In particular, we considered four classes: (i) active/reactivated/suspended landslides, (ii) dormant landslides, (iii) inactive/stabilized landslides, and (iv) area affected by widespread shallow landslides. In stable areas, certainly or supposed, we set two further classes based on a buffer zone of 50 m from the boundaries of mapped landslides (Figure 5A).

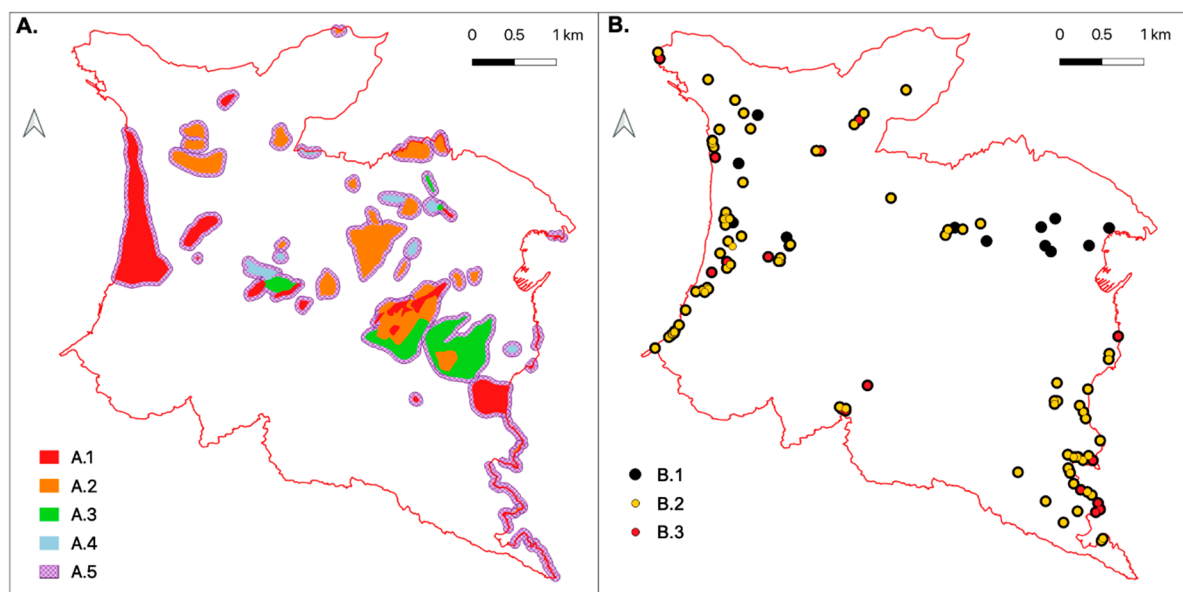


Figure 5. (A) Existing landslides, IFFI Project (Regione Liguria, 2014): 1. Active/reactivate/pendent landslide; 2. Dormant landslide; 3. Inactive/stabilised landslide; 4. Area affected by widespread shallow landslides; 5. Buffer zone (50 m). (B) Spatial distribution of gathered rainfall-induced shallow landslides over the 1910–2019 period: 1. Complete set. 2. Training set. 3. Test set.

2.4. Analytic Hierarchy Process (AHP)

To assess the landslide susceptibility of the Portofino promontory combining all the variables, we adopted the Analytic Hierarchy Processes (AHP) developed by Saaty [91], a semi-quantitative multi-criteria decision-making approach which enables to compute rank and weight of each criterion by a pair-wise comparison.

This approach includes several steps: (i) break a composite unstructured problem down into its component factors n and arrange them in a hierarchic order; (ii) assign numerical values according to the subjective relevance of each factor to determine its relative importance by a matrix-based pair-wise comparison

$$A = \|a_{(i,j)}\|, \quad (1)$$

where $i, j = (1, 2, \dots, n)$; (iii) synthesize the rating to determine the priority ω_n , i.e., the weight, to be assigned to each factor computing the normalized principal eigenvector λ_{max} , which corresponds to the largest eigenvalue [92,93]. In the pair-wise comparison, a scale of preference alternatives is used to associate a score based on the subjective judgment on the relative importance of each factor against every other one (Table 3).

Table 3. Scale of preference between two criteria used in the pair-wise comparison in AHP [88].

Scale	Degree of Preference	Description
1	Equally	Two factors contribute equally to the objective
3	Moderately	Experience and judgment slightly to moderately favor one factor over another
5	Strongly	Experience and judgment strongly or essentially favor one factor over another
7	Very strongly	A factor is strongly favored over another and its dominance is showed in practice
9	Extremely	The evidence of favoring one factor over another is of the highest degree possible of an affirmation
2,4,6,8	Intermediate	Used to represent compromises between the preferences in weights 1, 3, 5, 7 and 9
Reciprocals	Opposite	Used for inverse comparison

In this study, the nine considered variables influencing shallow landslides represent the component factors of the unstructured composite problem required by the method. To analyze the correlations between the conditioning factors and the landslides that occurred in the study area and arrange them in a hierarchic order, we firstly performed a simple frequency distribution analysis for each conditioning factor and for the different classes within each of them (Table 2). For this purpose, according to Chung and Fabbri [94] and Carrara et al. [95], we considered a portion of the gathered landslide inventory to evaluate the proneness to shallow landslide (training set), using the remaining landslides data to validate the resulting susceptibility model (test set) (Figure 5B). The training set has been defined by selecting randomly [9] 80% of the georeferenced landslides with a geographical accuracy <10 km² (P1 and P2).

Next, with respect to their impact on slope stability, we performed the pair-wise comparison for each conditioning factor and for the different classes within each factor using the AHP Excel template [96]. The template, which works under Excel version MS Excel 2013, can solve and combine the matrix of pair-wise comparisons of a maximum number of ten criteria computed by a maximum number of twenty experts. In this work, we used this approach to combine AHP results computed by five participants. The AHP Excel template includes (i) twenty input worksheets for pair-wise comparisons, where priorities are calculated using the row geometric mean method (RGMM); (ii) a sheet for the consolidation of all judgments, where weights given in the input sheets by individual par-

ticipant are aggregated using the Weighted Geometric Mean (WGM); and a (iii) summary sheet to display the consolidated final results for all the experts.

Final results include (i) weights of all considered criteria and associated errors (in %); (ii) principal or largest eigenvalue λ_{max} of the matrix, and (iii) a modified consistency ratio CR as proposed by Alonso and Lamata [97], calculated in all input sheets and in the summary sheets. The consistency ratio CR is an index ranging from 0 to 1, used to determine the degree of matrix consistency; it has been defined by Saaty [92] as the ratio between the calculated consistency index of the matrix CI and a random consistency index RI.

The consistency index CI estimates the consistency of weights and ratings and it is calculated based on Saaty's [98] expression:

$$CI = (\lambda_{max} - n) / (n - 1), \quad (2)$$

where λ_{max} is the largest eigenvalue and n is the order of the matrix, corresponding to the number of parameters.

The random consistency index RI, reported by Saaty [92] as the average of the resulting consistency index depending on the order of the matrix, in the AHP Excel Template adopted in the present study is calculated using the Alonso and Lamata linear fit [97], which estimates the RI as the best adjustment fit of the values of $\bar{\lambda}_{max}(n)$:

$$\bar{\lambda}_{max}(n) = 2.7699n - 4.3513, \quad (3)$$

where $\bar{\lambda}_{max}$ is the mean of λ_{max} .

The CR is therefore calculated by the following expression:

$$CR = (\lambda_{max} - n) / (2.7699n - 4.3513 - n) \quad (4)$$

Value of CR smaller than or equal to 0.1 (10%) is acceptable and, consequently, the matrix is consistent.

An AHP consensus indicator S^* is also calculated to quantify the consensus of the group, i.e., to estimate the agreement on the outcoming priorities between all the experts and it can be interpreted as a measure of overlap between priorities of the group members. This indicator is calculated using the partitioning diversity in Alpha and Beta diversity [99] derived from the Shannon entropy [100]. The consensus indicator S^* ranges from 0% (no consensus between experts) to 100% (full consensus between experts): values below 50% indicate a very low consensus, i.e., a high diversity of judgments, whereas values ranging from 80% to 90% indicate a high overlap of priorities and an excellent agreement of judgments from the group members.

2.5. Landslide Susceptibility Map

Once coherent weights have been assigned to each landslide causal factor and to each class within conditioning factor performing the AHP approach, all thematic vector layers have been converted into grid format with a 5×5 m cell size using the GRASS 7 (Geographic Resources Analysis Support System) native plugin in QGIS. Next, the reclassification of all grid data by weight values has been performed using the SAGA (System for Automated Geoscientific Analysis) reclassify values algorithm in QGIS.

A raster analysis has been performed to construct the landslide susceptibility map (LSM) using the Raster Calculator tool in QGIS. All the weighted predisposing factors and their classes have been combined using a weighted linear sum and then normalized by scaling values between 0 and 1 using the maximum value for the calculated variable:

$$LSM = (\sum_{i=1}^n w_{ij} W_j) / (\sum_{i=1}^n w_{ij} W_j)_{max}, \quad (5)$$

where w_{ij} is the weight factors of the class i in the conditioning factors j , W_j is the weight of the landslide conditioning factor j . Lastly, values resulting from the raster analysis have

been classified into 5 classes (low, moderate, high and very high) based on the histogram classification to determine the interval of each landslide susceptibility class in the map.

3. Results

We identified 85 rainfall events and 114 landslides in the 1910–2019 period. More than 50% of the observed instability processes involved the western and south-western sectors of the promontory, within the Camogli municipality, followed by Santa Margherita Ligure (30%) and Portofino (16%) (Figure 6A). Shallow landslides (43%) and rock falls (30%) are the most representative type of rainfall-induced rapid mass movements. Debris and mud flows occur with less frequency (<10%) (Figure 6B).

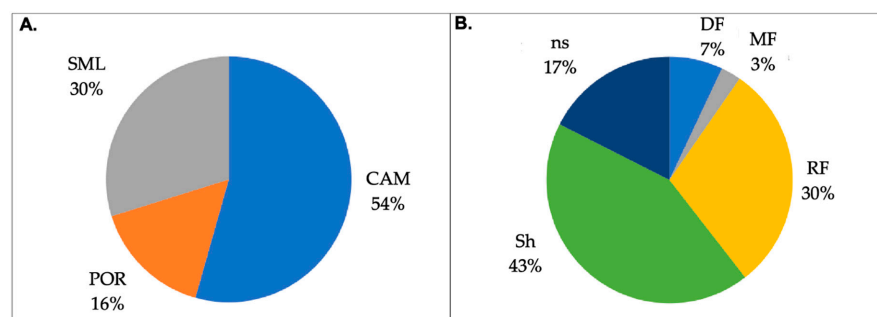


Figure 6. (A) Distribution of rainfall-induced shallow landslides in the Portofino promontory: CAM, Camogli municipality; POR, Portofino municipality; SML, Santa Margherita Ligure municipality (for location, see Figure 1). (B) Type of rainfall-induced shallow landslides within the Portofino promontory: DF, debris flow; MF, mud flow; ns, not specified; RF, rock fall; Sh, shallow landslide.

Results of the landslides spatial analysis show that slope failures occurred mainly in marly limestone with shale interlayers (48%) and conglomerate (41%), whereas incoherent soils and heterogeneous materials of anthropic origin are involved less frequently (8% and 3% respectively). With respect to the morphometric parameters, mass movements induced by rainfall affected mainly slopes of east (21%), north-west (20%) and west (18%) direction; south-west (13%) and north-east (11%) are also relevant slope directions, whereas north and south-east directions (5% respectively) are no representative. Landslides triggered mainly on slopes with high and very high steepness values (70%), higher than 50%. Most of instability processes developed within vegetated areas, characterized by mixed forests (26%), olive groves (26%) and broad-leaved forests (20%). Regarding urbanized areas, landslides have been detected largely on slopes with a discontinuous urban fabric (15%). Only 1% of gravitational processes involved bare rocks. Half of the observed landslides affected terraced slopes (50%), made of dry-stone walls terraces or grassy embankments, both well-maintained and abandoned.

With respect to the existing landslides mapped in the regional master plans, we found that most of the rainfall-induced failures (80%) involved slopes where no landslides have been previously detected. Only in 20% of cases, they match with existing landslides, classified as active/reactivated/suspended (16%) and dormant (4%); this percentage increases to 45% if we consider a buffer of 50 m around the landslide features. Similarly, in few cases landslides occurred within 10 m from watercourses (11%) or within 5 m from man-made cuts and structures, including main roads (9%), trails (11%), buildings (21%), manufacts (7%) and retaining walls (27%).

Among the 114 landslides, we considered 102 processes for which geographical location was known with a high or medium spatial accuracy (P1 and P2). The training set used to assess the landslide susceptibility consists of 81 landslides.

As proposed by the AHP method, the pairwise comparison matrix has been constructed both between the nine landslide causal factors and between the classes within each of them. In order to assess their impact on slope stability, each variable has been rated against every other by assigning a relative dominant value between 1 and 9 to the intersecting cell based

on the results of the frequency analysis performed using the random selected landslide training set. Table 4 summarizes normalized principal eigenvectors and associated errors for conditioning factors. Complete pairwise comparison matrixes for causal factors and for the classes within each landslide conditioning factor are shown in Appendices A–C.

Table 4. Summary of AHP analysis [96] computed by five participants: normalized principal eigenvector value and associated errors for landslide conditioning factors.

Factor	Number of Criteria	Normalized Principal Eigenvector	Error
Lithology	5	0.155	0.076
Aspect	9	0.090	0.040
Acclivity	7	0.311	0.107
Land use	10	0.197	0.093
Terraced area	2	0.064	0.033
Distance hydrographic elements	4	0.034	0.015
Distance man-made cuts	4	0.031	0.015
Distance man-made structures	4	0.055	0.003
Existing landslides	6	0.063	0.024

Calculated weights for the landslide conditioning factors range between 0.031 and 0.311: getting the highest value, slope acclivity represents the most relevant factor in the initiation of shallow landslides on the Portofino promontory, followed by land use (0.197) and lithology (0.155). Contrariwise, distance from hydrographic elements and man-made cuts slightly influence the landslide occurrence, weighting 0.034 and 0.031 respectively. By considering the different classes within each conditioning factor (Appendices B and C), the lithological features more predisposing to instability are limestone flysch (0.507) and conglomerate (0.308), whereas low weights have resulted for incoherent soils (0.04) and heterogeneous materials of anthropic origin (0.022). Regarding the morphometric conditioning factors, the highest weights have been assigned to slopes facing NW (0.285) and E (0.248) respectively and slope acclivity values ranging between 51% and 75% (0.331); medium weights to slope oriented to W (0.144) and SW (0.111) and steepness range values ranging from 76% to 100% (0.221) and higher 100% (0.202) respectively; lowest weights to the remaining morphometric classes. For land use, forest (0.358) is the more predisposing class to shallow landslides initiation, followed by permanent crops (0.204) and urban fabric (0.150); similarly, presence of terraces greatly influences the landslides occurrence (0.739). Weights result proportionally to the distance of landslides from the hydrographic network (0.394), man-made cuts (0.672) and anthropic structures (0.540): the farthest buffer zones had the higher assigned weights. Regarding pre-existing landslides, the highest scores have been assigned to area where no former gravitation processes have been mapped within the buffer zone higher (0.423) and lower (0.300) than 50 m from the existing landslide boundaries.

Consistency of the weights and rating calculated for each conditioning factors and the agreement on the outcoming priorities between all the participants are shown in Table 5. Values of the Consistency Ratio index (CR) are smaller than 10%, confirming that all the constructed matrixes are consistent: excepting for lithology (9.2%), CR values range from 0.0% (presence of terraced areas) to 5.2% (presence of existing landslides). Consensus indicator (S*) values reported in Table 5, ranging from 94.6% and 99.0%, show a very good consensus between the members of the research team.

Combining weightage of conditioning factors and their classes, we obtained the landslide susceptibility map of the Portofino promontory. We normalized the resulting LSM values, which ranged from 0.079 to 0.401, by scaling values between 0 and 1. In order to determine the class intervals in the obtained map, we took into consideration the classification systems commonly applied in landslide susceptibility zonation: natural breaks, quantiles and equal intervals [101]. On the basis of the raster map histogram, which is multimodal and shows empty class intervals, we adopted the natural breaks method to divide the LSM values into five classes shown in Table 6. In this case, the quantile

classification is not appropriate because data are not linearly distributed; whereas the lowest susceptibility class is too emphasized relative to others using equal intervals.

Table 5. Number of criteria considered for each landslide conditioning factor, Eigenvalue λ , consistency ratio, CR [97] and consensus indicator, S^* [96].

Factors	Number of Criteria	Eigenvalue λ	CR (%)	S^* (%)
Lithology	5	5.413	9.2	99.0
Aspect	9	9.480	4.1	97.9
Acclivity	7	7.296	3.7	95.6
Land use	10	10.330	2.5	94.9
Terraced areas	2	2.000	0.0	96.7
Distance hydrographic elements	4	4.068	2.5	96.9
Distance man-made cuts	4	4.035	1.3	94.6
Distance man-made structures	4	4.064	2.3	96.5
Existing landslides	6	6.329	5.2	98.9

Table 6. Landslide susceptibility classes and correlated LSM range value.

Class	LSM Range
Very low	0.00–0.40
Low	0.41–0.55
Medium	0.56–0.65
High	0.66–0.75
Very high	0.76–1.00

The resulting landslide susceptibility map for the Portofino promontory is presented in Figure 7A. Most of the territory (74%) results prone to shallow landslide occurrence: the highest extension percentage (30%) falls into moderate landslide susceptibility class, followed by high (26%) and very high (18%) susceptibility classes (Figure 7B). Otherwise, a small portion of the study area (26%) has been classified with low and very low landslide susceptibility.

We observed that areas with the highest proneness to rapid and very rapid mass movements occurrence (class = 5) comprise primarily the southern sectors of the promontory, where bedrock mainly consists of flysch (57%) and, secondarily, of conglomerate (30%), and slopes have a prevalent E (21%) and SE (14%) exposure, with high and very high steepness values (43%) comprised between 51% and higher than 101%. Sectors with high to very high landslide susceptibility are largely covered by forests (45%), permanent crops (34%) and shrubs or other natural vegetation (11%), with large areas characterized by outcropping bedrock, particularly along the high cliffs. Furthermore, they show the lowest interaction with anthropic elements, including roads (12%), buildings (6%), man-made structures (5%) and terraces (7%), and with pre-existing gravitational processes (1%).

Validation of the landslide susceptibility map has been performed on the basis of the test set consisting of 20 randomly selected landslide locations [94]. The distribution of landslides in the five LSM classes represents the qualitative assessment of the susceptibility map: we found that most of the landslides (65%) fell within the very high and the high susceptibility classes (35% and 30% respectively), confirming the strong connection between the occurrence of rainfall-induced rapid mass movements and the produced susceptibility zonation. A quantitative assessment of the predictive accuracy of the map has been computed using the Receiver Operating Characteristic curve (ROC) and the Area Under Curve (AUC) [35,102]. For this purpose, we plotted the true positive rate (TPR), i.e., the correctly predicted events, opposite to the false positive rate (FPR), i.e., the falsely predicted events, by varying the cut-off value. The prediction curve shows that the AUC value was 0.73 (Figure 8). According to Sewts [103], the quantitative relationship between the AUC value and the accuracy of the predictive model is classified as weak (0.5–0.6), moderate (0.6–0.7), good (0.7–0.8), very good (0.8–0.9) and excellent (0.9–1.0). Therefore, the proposed

landslide susceptibility map had a good prediction accuracy in rapid mass movements occurrence in the study area, when considering all the considered causative factors.

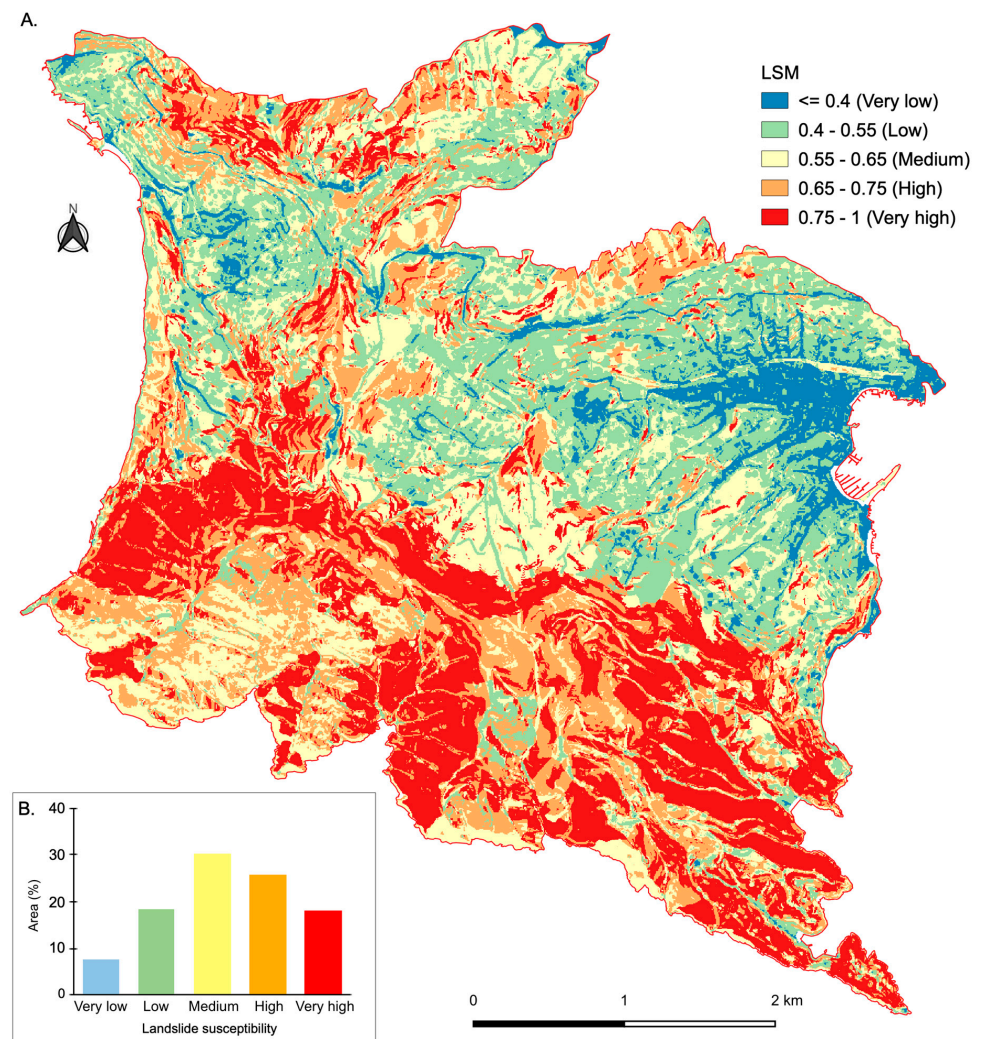


Figure 7. (A) Landslide susceptibility map of the Portofino promontory. (B) Histogram of the percentage of areas included in the five susceptibility classes.

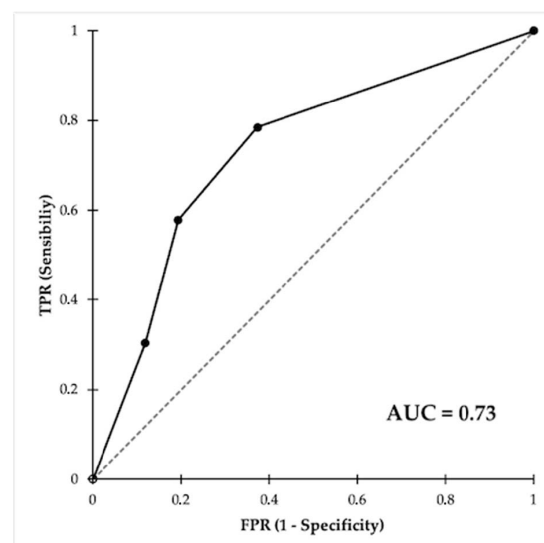


Figure 8. Predictive accuracy of the proposed landslide susceptibility model using the ROC curve.

4. Discussion

The landslide susceptibility map obtained through the AHP semi-quantitative approach (Figure 9A) represents a great tool for risk mitigation planning. The proposed methodology, already applied in similar geographical and geological context, combines an objective and quantitative component with a degree of subjectivity that arises from the experts' judgement, which are properly mediated through the AHP method. Then, the subjectivity level, although reduced in importance, allows one to introduce the experts' opinion in the decision-making process. The result is a susceptibility map that combines the experts' opinions and the objective record of past events.

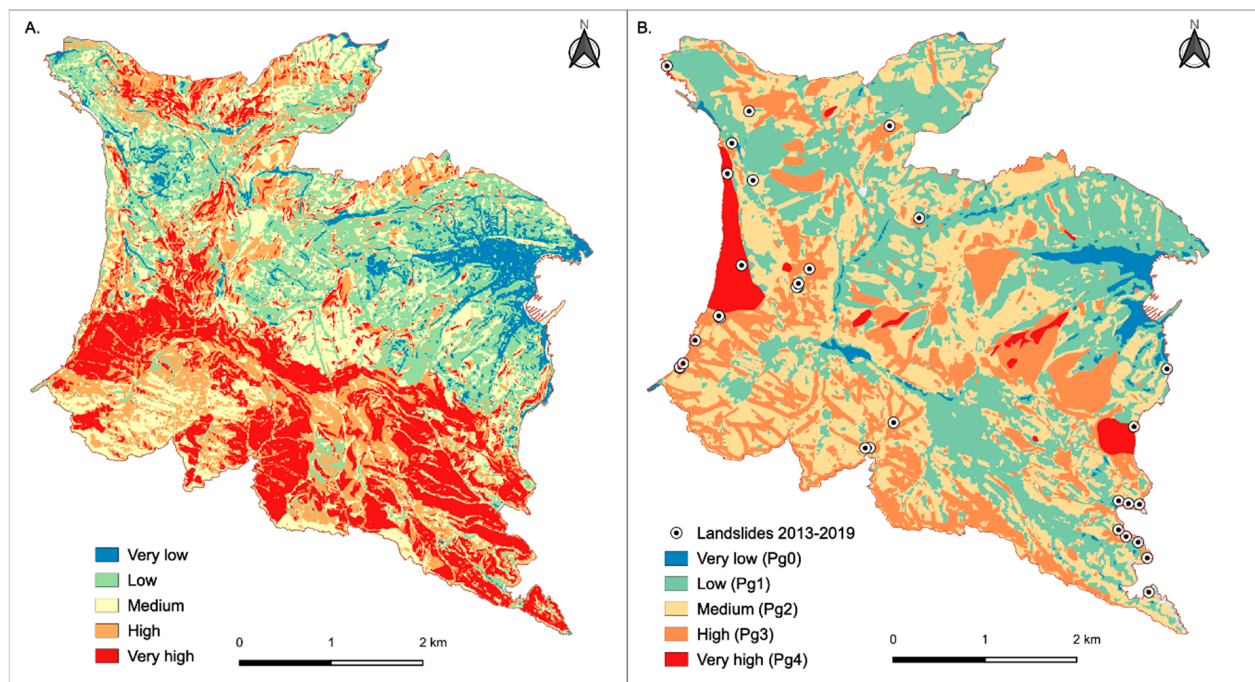


Figure 9. Comparison between: (A) the proposed landslide susceptibility map, and (B) the landslide susceptibility zonation currently adopted by the regional land and risk management plan. Black dots represent rainfall induced landslides which occurred after 2013.

Actually, the river basin management plan (defined Basin Master Plan) [104] adopts a different methodology to obtain the landslide susceptibility map (Figure 9B). The methodology, which derives from a specific technical regulation, includes some conditioning factors at the catchment's scale: lithology, slope steepness, land use, hydrological effectiveness, soil cover and related granulometry and the presence of active or inactive landslides. Some other worsening factors are then included, e.g., lithological contact, fault, erosional talweg channel, edge of fluvial erosion scarp, terrace edge, slope angle discontinuity. Weights within every factor are assigned subjectively, apart from lithology where a statistical approach is used, considering the proportion of in landslide lithotype. Maps are summed up, and after normalization, susceptibility classes are assigned. Then, the methodology is highly affected by subjectivity and strongly relies on the presence of active and inactive landslides. Conditioning factors at local scale, including man-made landforms, are not included in the assessment of landslide susceptibility. Furthermore, areas where active, dormant or inactive/stabilized landslide, deep seated gravitational slope deformation, widespread active or dormant instability phenomena and shallow landslides are detected, are automatically classified as high or very high susceptibility zones. The obtained map is classed in 5 increasing levels of susceptibility, named from Pg0 to Pg4 (Figure 9B).

We observed that areas with very high landslides susceptibility overlap effectively with existing active mapped landslides; similarly, slopes with high susceptibility are largely affected by existing dormant or inactive landslide.

The comparison between the regional susceptibility zonation and the spatial distribution of rainfall-induced shallow landslides occurred in the Portofino promontory after 2013, which is the year of publication of the regional map, shows that most of them affected slopes classified as medium (Pg2) susceptibility. This result highlights the unreliability of the previous model to map landslide susceptibility for predicting areas where new slope failures may occur, as it probably relies too much on the existing phenomena in terms of their geometrical features, and less on the conditioning factors.

The differences between the previous model and the proposed one (Figure 9) are particularly relevant in the southern part of the area, whose lithology is conglomerate, which is characterized by strong steepness. This factor, in the studied area, is probably the crucial one but it is primarily accompanied by man-made landforms and hydrographical network, and then by the others. The proposed model probably underestimates the presence of existing large landslides, but this apparent limitation may be easily overcome, adopting the same method of the actual in-use model, which automatically assigns the highest class to active landslide zones (Figure 10). In fact, it is surely true that active landslides represent risk elements themselves and may result, in some local portions, as a possible source of rapid mass movements.

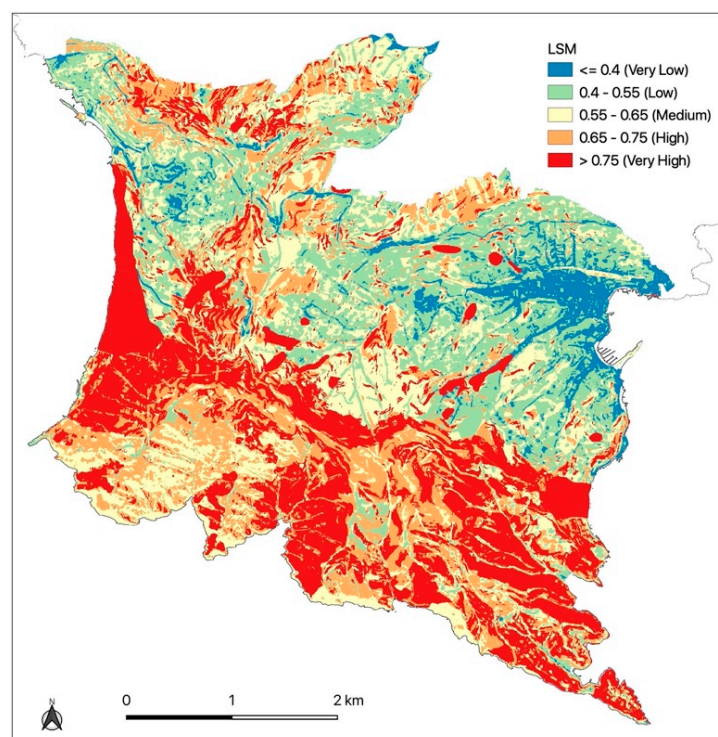


Figure 10. The obtained susceptibility map with automatic assignment of the highest class to existing active landslides zones and areas affected by widespread shallow landslides.

The comparison between the proposed susceptibility map (Figure 10) and the regional susceptibility zonation (Figure 9B) has been performed through Cohen's Kappa calculation [105,106], using the Map comparison kit software, version 3.2.3 [107]. The obtained Kappa value was 0.108, and the correct fraction was 0.308, showing a general slight concordance between the two maps. Results per susceptibility class are shown in Table 7: medium and high classes displayed the lowest and no concordance, respectively, while the very low one presented a relatively higher degree of concordance, confirming the general result even if differentiating between classes. The lowest susceptibility class

corresponded substantially with the lower slope gradient areas, that is the lower values of the more critical conditioning factor. On the other hand, the weak concordance in the three higher susceptibility classes highlights the strong differentiation between the two maps where landslide triggering probability is higher.

Table 7. Kappa per susceptibility class map comparison between regional zonation and the proposed one.

Class	Very Low	Low	Medium	High	Very High
Kappa	0.322	0.185	0.044	−0.014	0.173

Then, the proposed susceptibility map (Figure 10), modifying landslides area zonation, may be intended as a more effective and efficient tool to support risk mitigation strategies and planning. More accurate knowledge of where a future possible landslide may occur allows us to eventually reduce the importance of critical man-induced factors and to promote proper prevention measures that are crucial for reducing damage and even victims [39,108,109].

5. Conclusions

The research allowed us to assess a landslide susceptibility map for the Portofino promontory, based on over 110 years of rapid mass movements inventory and experts' opinions, to apply a semi-quantitative AHP method. Then, the methodology combines the quantitative approach with an expert-based view. The analysis of nine conditioning factors, which includes anthropogenic landforms related ones, results in a susceptibility map that highlights areas where possible future landslides may occur with a reliability that appears higher than the one of the actual officially adopted map. The way the proposed map has been compiled seems more oriented towards the possible future landslide scenario, rather than weighting the existing landslides with higher importance.

Then, the proposed map results as a possible decision support tool to implement risk mitigation strategies and to better apply land use planning in an area that is periodically hit by intense rain events that often induce rapid mass movements. The combination of those types of landslides and flash flood often occurs, causing the culverts saturation in urban and peri-urban areas and resulting in large damage. The RECONNECT EU funded project is actually adopting risk mitigation strategies for slope stabilization in the studied area and a susceptibility map is a crucial decision support tool for interventions planning [110].

Finally, the methodology allows us to modify factors, including new ones or excluding others, in order to localize features, and it may then be adopted in different conditions or geographical contexts.

Author Contributions: Conceptualization, A.R. and G.P.; methodology, A.R. and G.P.; software A.R. and G.P.; validation, A.R., G.P. and F.F.; investigation, A.R.; resources, A.R. and G.P.; data curation, F.F., F.L. and L.T.; writing—original draft preparation, A.R. and G.P.; writing—review and editing, A.R., F.F. and L.T.; visualization, A.R., G.P., F.L. and L.T.; supervision, G.P. and L.T.; project administration, F.L. and L.T. All authors have read and agreed to the published version of the manuscript.

Funding: This article is an outcome of the RECONNECT project (Regenerating ECOsystems with Nature-based solutions for hydro-meteorological risks eEduCTion). This project received funding from the European Union's Horizon 2020 research and Innovation Program under grant agreement No. 776866.

Institutional Review Board Statement: Not applicable.

Informed Consent Statement: Not applicable.

Acknowledgments: The authors wish to thank Riccardo Buelli, Benedetto Mortola and Francesco Olivari for the support, the data provided and the useful discussion on landslide of Portofino's Promontory.

Conflicts of Interest: The authors declare no conflict of interest.

Appendix A

Summary of AHP analysis: pairwise comparison matrix computed by five participants, normalized principal eigenvector value and associated errors for landslide conditioning factors.

Factor	1	2	3	4	5	6	7	8	9	Normalized Principal Eigenvector	Error
Lithology	1	3 3/4	2/7	1/3	2 2/5	2 8/9	5 3/4	3 4/5	3 2/3	0.155	0.076
Aspect	1/4	1	1/4	3/8	2	2 1/4	2 3/8	2 1/7	3	0.090	0.040
Acclivity	3 4/7	3 3/4	1	2 5/9	4 1/3	7	7	6 1/8	4 1/8	0.311	0.107
Land use	2 3/4	2 3/5	2/5	1	2 3/5	3	4 1/2	4 1/2	4 1/2	0.197	0.093
Terraced area	2/5	1/2	1/4	3/8	1	4 2/7	3 1/4	4/9	5/9	0.064	0.033
Distance hydrographic elements	1/3	4/9	1/7	1/3	1/4	1	7/9	5/9	3/8	0.034	0.015
Distance man-made cuts	1/6	3/7	1/7	2/9	1/3	1 2/7	1	5/8	3/8	0.031	0.015
Distance man-made structures	1/4	1/2	1/6	2/9	2 2/9	1 4/5	1 3/5	1	3/4	0.055	0.003
Existing landslides	2/7	1/3	1/4	2/9	1 7/9	2 3/5	2 3/5	1 1/3	1	0.063	0.024

Appendix B

Summary of AHP analysis: pairwise comparison matrix computed by five participants, normalized principal eigenvector value and associated errors for the classes within each landslide conditioning factor.

Factor Classes	1	2	3	4	5	6	7	8	9	10	Normalized Principal Eigenvector	Error
						<i>Lithology</i>						
Alluvial deposits	1	1/5	2/7	1/8	1/8						0.031	0.016
Slope covers	5	1	2 1/6	1/7	1/6						0.093	0.040
Fills	3 3/8	1/2	1	1/7	1/6						0.061	0.022
Flysch	8 1/3	7 1/6	7 1/9	1	2 6/7						0.507	0.218
Conglomerate	7 3/4	6 1/5	6	1/3	1						0.308	0.140

Factor Classes	1	2	3	4	5	6	7	8	9	10	Normalized Principal Eigenvector	Error
<i>Aspect</i>												
N	1	1/3	1/5	1 1/7	2/7	2/9	1/6	1/8	2 5/9		0.318	0.012
NE	3	1	1/4	2 3/8	1	2/5	2/7	1/6	4 1/2		0.617	0.020
E	5	4 1/3	1	6 1/2	5	3 2/7	2 3/4	3/4	7		0.247	0.081
SE	7/8	3/7	1/7	1	1/3	2/7	2/7	1/4	1 8/9		0.355	0.014
S	3 3/8	1	1/5	2 3/4	1	3/8	1/3	1/5	3 2/7		0.628	0.021
SW	4 4/7	2 1/2	1/3	3 1/3	2 5/7	1	5/9	2/7	5 1/3		0.111	0.033
W	5 4/7	3 3/5	1/3	3 1/3	3	1 7/9	1	1/3	6 1/7		0.144	0.046
NW	7 3/4	6 1/7	1 1/3	4	4 5/6	3 2/3	3 1/9	1	8 1/6		0.285	0.098
Zenith	2/5	2/9	1/7	1/2	1/3	1/5	1/6	1/8	1		0.021	0.008
<i>Acclivity</i>												
0–10%	1	1	1/4	1/4	1/7	1/5	1/5				0.033	0.010
11–20%	1	1	1/4	1/4	1/6	1/5	1/6				0.033	0.011
21–35%	4 1/3	4 1/8	1	1	1/4	2/7	2/7				0.090	0.032
36–50%	4 1/8	4	1	1	1/4	2/7	1/3				0.090	0.027
51–75%	6 4/7	6	4	4	1	2	2 1/3				0.331	0.102
76–100%	5 2/5	5 1/2	3 2/3	3 4/9	1/2	1	1 1/7				0.221	0.064
>100%	5 2/9	5 2/3	3 4/9	3	3/7	7/8	1				0.202	0.057

Appendix C

Factor Classes	1	2	3	4	5	6	7	8	9	10	Normalized Principal Eigenvector	Error
<i>Land Use</i>												
Urban fabric	1	5	3 5/8	5	2/5	4 8/9	4 1/2	1/5	3 1/4	4 4/7	0.149	0.042
Industrial/commercial/ transport units	1/5	1	1 1/7	1 1/3	2/9	2/3	1	1/7	4/9	1 1/7	0.038	0.009
Artificial non-agricultural areas	2/7	7/8	1	1 1/7	1/5	1 1/2	1 1/7	1/7	1/2	1 1/7	0.041	0.006
Arable land	1/5	3/4	7/8	1	1/6	1 1/3	3/4	1/7	3/5	3/5	0.034	0.008

Factor Classes	1	2	3	4	5	6	7	8	9	10	Normalized Principal Eigenvector	Error
Permanent crops	2 1/2	4 5/9	5	5 1/2	1	5 1/8	4 3/4	1/3	4 2/9	5 5/9	0.204	0.067
Pastures	1/5	1 3/7	2/3	3/4	1/5	1	7/8	1/7	2/5	2/3	0.034	0.011
Heterogeneous agricultural areas	2/9	1	7/8	1 1/3	1/5	1 1/7	1	1/7	1/2	1	0.038	0.006
Forests	4 3/4	7 1/9	6 5/7	6 5/7	3	6 5/7	7 1/4	1	7	7 1/3	0.358	0.164
Shrubs ecc.	1/3	2 2/9	1 8/9	1 2/3	1/4	2 5/9	2 1/6	1/7	1	1 3/4	0.064	0.015
Open space with little/no vegetation	2/9	7/8	7/8	1 2/3	1/6	1 1/2	1	1/7	4/7	1	0.040	0.008
Terraced areas												
Area with terraces	1	1/3									0.261	-
Area without terraces	2 5/6	1									0.739	-
Hydrographic elements distance												
Watercourses, d > 10m	1	6 1/3	2/3		6 6/7						0.394	0.077
Watercourses, d < 10m	1/6	1	1/6		2						0.081	0.002
Springs, d > 10 m	1 3/7	6 1/3	1		6 6/7						0.471	0.081
Springs, d < 10 m	1/7	1/2	1/7		1						0.054	0.012
Man-made cuts distance												
Man-made cuts, d > 5 m	1	6 1/2	5 4/7		6 3/4						0.672	0.119
Trails, d < 5 m	1/7	1	1 1/7		1 7/9						0.127	0.018
Main roads, d < 5 m	1/6	7/8	1		1 7/9						0.122	0.013
Minor roads, d < 5 m	1/7	5/9	5/9		1						0.79	0.014
Man-made structures distances												
Man-made structures, d > 10 m	1	3 8/9	5 2/9		2 5/6						0.540	0.104
Buildings, d < 10 m	1/4	1	2 5/6		3/5						0.160	0.038
Other manufacts, d < 10 m	1/5	1/3	1		1/3						0.077	0.019
Retaining walls, d < 10 m	1/3	1 2/3	3		1						0.222	0.029

Factor Classes	1	2	3	4	5	6	7	8	9	10	Normalized Principal Eigenvector	Error
<i>Existing landslides (IFFI Project)</i>												
Inactive/stabilized	1	1/2	2/9	1 1/2	1/7	1/6					0.044	0.015
Dormant	2 1/6	1	1/3	1 1/3	1/6	1/5					0.060	0.017
Active/reactivated/ suspended	4 4/7	3 1/9	1	4 3/8	1/5	1/4					0.133	0.053
Area affected by widespread shallow landslides	2/3	3/4	2/9	1	1/7	1/6					0.040	0.012
Assumed stable area, d > 50 m	6 2/3	6 1/7	5 1/3	6 2/3	1	2					0.423	0.171
Assumed stable area, d < 50 m	5 7/9	5 1/7	4 2/7	6 4/9	1/2	1					0.300	0.123

References

- Heersink, P. World Atlas of natural hazards. *Cartographica* **2005**, *40*, 133–134. [\[CrossRef\]](#)
- Petley, D. Global patterns of loss of life from landslides. *Geology* **2012**, *40*, 927–930. [\[CrossRef\]](#)
- Froude, M.J.; Petley, D.N. Global fatal landslide occurrence from 2004 to 2016. *Nat. Hazards Earth Syst. Sci.* **2018**, *18*, 2161–2181. [\[CrossRef\]](#)
- Haque, U.; da Silva, P.F.; Devoli, G.; Pilz, J.; Zhao, B.; Khaloua, A.; Wilopo, W.; Andersen, P.; Lu, P.; Lee, J.; et al. The human cost of global warming: Deadly landslides and their triggers (1994–2014). *Sci. Total.* **2019**, *682*, 673–684. [\[CrossRef\]](#) [\[PubMed\]](#)
- Hungr, O.; Leroueil, S.; Picarelli, L. The Varnes classification of landslide types, an update. *Landslides* **2014**, *1*, 167–194. [\[CrossRef\]](#)
- Varnes, D.J. *Landslide Hazard. Zonation—A Review of Principles and Practice*; UNESCO: Paris, France, 1984; p. 63.
- Guzzetti, F.; Carrara, A.; Cardinali, M.; Reichenbach, P. Landslide hazard evaluation: A review of current techniques and their application in a multi-scale study, Central Italy. *Geomorphology* **1999**, *31*, 181–216. [\[CrossRef\]](#)
- Brabb, E.E. Innovative approaches to landslide hazard mapping. In Proceedings of the 4th International Landslides Symposium, Toronto, Canada, 16–21 September 1984; Volume 1, pp. 307–324.
- Pellicani, R.; Argentiero, I.; Spilotro, G. GIS-based predictive models for regional-scale landslide susceptibility assessment and risk mapping along road corridors. *Geomat. Nat. Haz. Risk* **2017**, *8*, 1012–1033. [\[CrossRef\]](#)
- Van Westen, C.J.; Van Asch, T.W.J.; Soeters, R. Landslide hazard and risk zonation: Why is it still so difficult? *Bull. Eng. Geol. Environ.* **2006**, *65*, 167–184. [\[CrossRef\]](#)
- Dai, F.C.; Lee, C.F.; Ngai, Y.Y. Landslide risk assessment and management: An overview. *Eng. Geol.* **2002**, *64*, 65–87. [\[CrossRef\]](#)
- Cascini, L.; Bonnard, C.; Corominas, J.; Jibson, R.; Montero-Olarte, J. Landslide hazard and risk zoning for urban planning and development. In *Landslide Risk Management*; Taylor and Francis: London, UK, 2005; pp. 199–235. [\[CrossRef\]](#)
- Corominas, J.; Van Westen, C.; Frattini, P. Recommendations for the quantitative analysis of landslide risk. *Bull. Eng. Geol. Environ.* **2014**, *73*, 209–263. [\[CrossRef\]](#)
- Brenning, A. Spatial prediction models for landslide hazards: Review, comparison and evaluation. *Nat. Hazards Earth Syst. Sci.* **2005**, *5*, 853–862. [\[CrossRef\]](#)
- Reichenbach, P.; Rossi, M.; Malamud, B.M.; Mihir, M.; Guzzetti, F. A review of statistically-based landslide susceptibility models. *Earth Sci. Rev.* **2018**, *180*, 60–91. [\[CrossRef\]](#)
- Yalcin, A.; Reis, S.; Aydinoglu, A.C.; Yomralioglu, T. A GIS-based comparative study of frequency ratio, analytical hierarchy process, bivariate statistics and logistics regression methods for landslide susceptibility mapping in Trabzon, NE Turkey. *Catena* **2011**, *85*, 274–287. [\[CrossRef\]](#)
- Turconi, L.; Luino, F.; Gussoni, M.; Faccini, F.; Giardino, M.; Casazza, M. Intrinsic Environmental Vulnerability as Shallow Landslide Susceptibility in Environmental Impact Assessment. *Sustainability* **2019**, *11*, 6285. [\[CrossRef\]](#)
- Dou, J.; Yunus, A.P.; Tien Bui, D.; Sahana, M.; Chen, C.W.; Zhu, Z.; Weidong, W.; Thai Pham, B. Evaluating GIS-based multiple statistical models and data mining for earthquake and rainfall-induced landslide susceptibility using the LiDAR DEM. *Remote Sens.* **2019**, *11*, 638. [\[CrossRef\]](#)
- Lai, J.-S.; Tsai, F. Improving GIS-based Landslide Susceptibility Assessments with Multi-temporal Remote Sensing and Machine Learning. *Sensors* **2019**, *19*, 3717. [\[CrossRef\]](#) [\[PubMed\]](#)
- Aleotti, P.; Chowdhury, R. Landslide hazard assessment: Summary review and new perspectives. *Bull. Eng. Geol. Environ.* **1999**, *58*, 21–44. [\[CrossRef\]](#)
- Fell, R.; Corominas, J.; Bonnard, C.; Cascini, L.; Leroi, E.; Savage, W.Z. Guidelines for landslide susceptibility, hazard and risk zoning for land use planning. *Eng. Geol.* **2008**, *102*, 85–98. [\[CrossRef\]](#)
- Van Westen, C.J.; Rengers, N.; Soeters, R. Use of Geomorphological Information in Indirect Landslide Susceptibility Assessment. *Nat. Hazards* **2003**, *30*, 399–419. [\[CrossRef\]](#)
- Van Den Eeckhaut, M.; Reichenbach, P.; Guzzetti, F.; Rossi, M.; Poesen, J. Combined landslide inventory and susceptibility assessment based on different mapping units: An example from the Flemish Ardennes, Belgium. *Nat. Hazards Earth Syst. Sci.* **2009**, *9*, 507–521. [\[CrossRef\]](#)
- Marsala, V.; Galli, A.; Paglia, G.; Miccadei, E. Landslide Susceptibility Assessment of Mauritius Island (Indian Ocean). *Geosciences* **2019**, *9*, 493. [\[CrossRef\]](#)
- Komac, M. A landslide susceptibility model using the analytical hierarchy process method and multivariate statistics in perialpine Slovenia. *Geomorphology* **2006**, *74*, 17–28. [\[CrossRef\]](#)
- Fan, W.; Wei, X.S.; Cao, Y.B.; Zheng, B. Landslide susceptibility assessment using the certainty factor and analytic hierarchy process. *J. Mt. Sci.* **2017**, *14*, 906–925. [\[CrossRef\]](#)
- Roccati, A.; Faccini, F.; Luino, F.; Ciampalini, A.; Turconi, L. Heavy Rainfall Triggering Shallow Landslides: A Susceptibility Assessment by a GIS-Approach in a Ligurian Apennine Catchment (Italy). *Water* **2019**, *11*, 605. [\[CrossRef\]](#)
- Montgomery, D.R.; Dietrich, W.E. A physically based model for the topographic control of shallow landsliding. *Water Resour. Res.* **1994**, *30*, 1153–1171.
- Lu, N.; Godt, J.W. Infinite-slope stability under steady un-saturated seepage conditions. *Water Resour. Res.* **2008**, *44*, W11404. [\[CrossRef\]](#)

30. Thiery, Y.; Vandromme, R.; Maquaire, O.; Bernardie, S. Landslide Susceptibility Assessment by EPBM (Expert Physically Based Model): Strategy of Calibration in Complex Environment. In *Advancing Culture of Living with Landslides; Workshop on World Landslide Forum 2017*; Mikos, M., Tiwari, B., Yin, Y., Sassa, K., Eds.; Springer: Cham, Switzerland, 2017; pp. 917–926. [\[CrossRef\]](#)
31. Lee, S.; Ryu, J.-H.; Won, J.-S.; Park, H.-J. Determination and application of the weights for landslide susceptibility mapping using an artificial neural network. *Eng. Geol.* **2004**, *71*, 289–302. [\[CrossRef\]](#)
32. Conforti, M.; Pascale, S.; Robustelli, G.; Sdao, F. Evaluation of prediction capability of the artificial neural networks for mapping landslide susceptibility in the Turbolo River catchment (northern Calabria, Italy). *Catena* **2014**, *113*, 236–250. [\[CrossRef\]](#)
33. Tsangaratos, P.; Loupasakis, C.; Nikolakopoulos, K.; Angelitsa, V.; Ilia, I. Developing a landslide susceptibility map based on remote sensing, fuzzy logic and expert knowledge of the Island of Lefkada, Greece. *Environ. Earth Sci.* **2018**, *77*, 363. [\[CrossRef\]](#)
34. Yalcin, A. GIS-based landslide susceptibility mapping using analytical hierarchy process and bivariate statistics in Ardesen (Turkey): Comparisons of results and confirmations. *Catena* **2008**, *72*, 1–12. [\[CrossRef\]](#)
35. Pourghasemi, H.R.; Pradhan, B.; Gokceoglu, C. Application of fuzzy logic and analytical hierarchy process (AHP) to landslide susceptibility mapping at Haraz watershed, Iran. *Nat. Hazards* **2012**, *63*, 965–996. [\[CrossRef\]](#)
36. Cignetti, M.; Godone, D.; Giordan, D. Shallow landslide susceptibility, Rupinaro catchment, Liguria (northwestern Italy). *J. Maps* **2019**, *15*, 333–345. [\[CrossRef\]](#)
37. Panchal, S.; Shrivastava, A.K. Application of analytic hierarchy process in landslide susceptibility mapping at regional scale in GIS environment. *J. Stat. Manag. Syst.* **2020**, *23*, 199–206.
38. Gamper, C.D.; Thöni, M.; Weck-Hannemann, H. A conceptual approach to the use of Cost Benefit and Multi Criteria Analysis in natural hazard management. *Nat. Hazards Earth Syst. Sci.* **2006**, *6*, 293–302. [\[CrossRef\]](#)
39. Paliaga, G.; Faccini, F.; Luino, F.; Turconi, L. A spatial multicriteria prioritizing approach for geohydrological risk mitigation planning in small and densely urbanized Mediterranean basins. *Nat. Hazards Earth Syst. Sci.* **2019**, *19*, 53–69. [\[CrossRef\]](#)
40. Regione Liguria. Carta Geologica Regionale (CGR), Scala 1:25,000, Tav. 231.1, 231.4—Chiavari Recco. 2005. Available online: <https://geoportal.regione.liguria.it/catalogo/mappe.html> (accessed on 17 November 2020).
41. Faccini, F.; Piccazzo, M.; Robbiano, A.; Roccati, A. Applied geomorphological map of the Portofino municipal territory. *J. Map* **2012**, *4*, 451–462. [\[CrossRef\]](#)
42. Bonaria, V.; Faccini, F.; Galiano, I.C.; Sacchini, A. Hydrogeology of conglomerate fractured-rock aquifers: An example from the Portofino's Promontory (Italy). *Rend. Online Soc. Geol. Ital.* **2016**, *41*, 22–25. [\[CrossRef\]](#)
43. Corsi, B.; Elter, F.M.; Giammarino, S. Structural fabric of the Antola Unit (Riviera di Levante, Italy) and implications for its alpine versus apennine origin. *Ofioliti* **2001**, *26*, 1–8.
44. Levi, N.; Ellero, A.; Ottria, G.; Pandolfi, L. Polyrogenic deformation history recognized at very shallow structural levels: The case of the Antola Unit (Northern Apennine, Italy). *J. Struct. Geol.* **2006**, *28*, 1694–1709. [\[CrossRef\]](#)
45. Fanucci, F.; Nosengo, S. Rapporti tra neotettonica e fenomeni morfogenetici del versante marittimo dell'Appennino ligure e del margine continentale. *Boll. Soc. Geol. Ital.* **1979**, *96*, 41–51. (In Italian)
46. Faccini, F.; Piccazzo, M.; Robbiano, A. Natural hazards in San Fruttuoso of Camogli (Portofino Park, Italy): A case study of a debris flow in a coastal environment. *Ital. J. Geosci.* **2009**, *128*, 641–654. [\[CrossRef\]](#)
47. Brandolini, P.; Faccini, F.; Piccazzo, M. Geomorphological hazard and tourist vulnerability along Portofino Park trails (Italy). *Nat. Hazard Earth Syst. Sci.* **2009**, *6*, 563–571. [\[CrossRef\]](#)
48. Faccini, F.; Robbiano, A.; Sacchini, A. Geomorphologic hazard and intense rainfall: The case study of the Recco Stream Catchment (Eastern Liguria, Italy). *Nat. Hazard. Earth Syst. Sci.* **2012**, *12*, 893–903. [\[CrossRef\]](#)
49. Brandolini, P.; Faccini, F.; Pelfini, M.; Firpo, M. A complex landslide along the Eastern Liguria rocky coast (Italy). *Rend. Online Soc. Geol. Ital.* **2013**, *28*, 28–31.
50. Brandolini, P.; Faccini, F.; Robbiano, A.; Terranova, R. Geomorphological hazards and monitoring activity along the western rocky coast of the Portofino Promontory (Italy). *Quater. Int.* **2006**, *171–172*, 131–142. [\[CrossRef\]](#)
51. Paliaga, G.; Luino, F.; Turconi, L.; De Graff, J.V.; Faccini, F. Terraced Landscapes on Portofino Promontory (Italy): Identification, Geo-Hydrological Hazard and Management. *Water* **2020**, *12*, 435. [\[CrossRef\]](#)
52. Food and Agricultural Organization of the United Nations—FAO. *World Reference Base for Soil Resources*, 2nd ed.; FAO: Rome, Italy, 2006. Available online: <http://www.fao.org/3/a-a0510e.pdf> (accessed on 17 November 2020).
53. Rellini, I.; Olivari, S.; Scopesi, C.; Firpo, M. The soils of the Portofino Promontory (Italy): Distribution, genesis and paleoenvironmental implications. *Geogr. Fis. E Din. Quat.* **2017**, *40*, 211–232.
54. Faccini, F.; Brandolini, P.; Robbiano, A.; Perasso, L.; Sola, A. Instability, precipitation phenomena and land planning: The flood of 2002 in lower Lavagna valley (Eastern Liguria, Italy). *Geogr. Fis. E Din. Quat.* **2005**, *Suppl. VII*, 145–153.
55. Anagnostopoulou, C.; Tolika, K.; Flocas, H.; Maheras, P. Cyclones in the Mediterranean region: Present and future climate scenarios derived from a general circulation model (HadAM3P). *Adv. Geosci.* **2006**, *7*, 9–14. [\[CrossRef\]](#)
56. Sacchini, A.; Ferraris, F.; Faccini, F.; Firpo, M. Environmental climatic maps of Liguria. *J. Maps* **2012**, *8*, 199–207. [\[CrossRef\]](#)
57. Paliaga, G.; Donadio, C.; Bernardi, M.; Faccini, F. High-resolution lightning detection and possible relationship with rainfall events over the Central Mediterranean Area. *Remote Sens.* **2019**, *11*, 1601. [\[CrossRef\]](#)
58. Acquavotta, F.; Faccini, F.; Fratianni, S.; Paliaga, G.; Sacchini, A.; Vilímek, V. Increased flash flooding in Genoa Metropolitan Area: A combination of climate changes and soil consumption? *Meteorol. Atmos. Phys.* **2019**, *131*, 1099–1110. [\[CrossRef\]](#)

59. Roccati, A.; Paliaga, G.; Luino, F.; Faccini, F.; Turconi, L. Rainfall threshold for shallow landslides initiation and analysis of long-term rainfall trends in a Mediterranean area. *Atmosphere* **2020**, *11*, 1367. [\[CrossRef\]](#)
60. Guzzetti, F.; Cardinali, M.; Reichenbach, P. The AVI Project: A bibliographical and archive inventory of landslides and floods in Italy. *Environ. Manag.* **1994**, *18*, 623–633. [\[CrossRef\]](#)
61. Hungr, O.; Evans, S.G.; Bovis, M.J.; Hutchinson, J.N. A review of the classification of landslides of the flow type. *Environ. Eng. Geosci.* **2001**, *7*, 221–238. [\[CrossRef\]](#)
62. European Environmental Agency—EEA. *CORINE Land Cover Technical Guide. Part 2: Nomenclature*; Office for Official Publications of the European Communities: Luxembourg, 1995.
63. Regione Liguria. Inventario dei Fenomeni Franosi Scale 1:10,000—Progetto IFFI (Last Update 2014). Available online: <https://geoportal.regione.liguria.it/catalogo/mappe.html> (accessed on 17 November 2020).
64. Faccini, F.; Gabellieri, N.; Paliaga, G.; Piana, P.; Angelini, S.; Coratza, P. Geoheritage map of the Portofino Natural Park (Italy). *J. Maps* **2018**, *14*, 87–96. [\[CrossRef\]](#)
65. Polemio, M.; Petrucci, O. Occurrence of landslide events and the role of climate in the twentieth century in Calabria, southern Italy. *Q. J. Eng. Geol. Hydrol.* **2010**, *43*, 403–415. [\[CrossRef\]](#)
66. Alexander, D. On the causes of landslides: Human activities, perception, and natural processes. *Environ. Geol. Water Sci.* **1992**, *20*, 165–179. [\[CrossRef\]](#)
67. Glade, T. Landslide occurrence as a response to land use change: A review of evidence from New Zealand. *Catena* **2003**, *51*, 297–314. [\[CrossRef\]](#)
68. Bruschi, V.M.; Bonachea, J.; Remondo, J.; Gomez-Arozamena, J.; Rivas, V.; Barbieri, M.; Capocchi, S.; Soldati, M.; Cendrero, A. Land management versus natural factors in land instability: Some examples in Northern Spain. *Environ. Manag.* **2013**, *52*, 398–416. [\[CrossRef\]](#)
69. Persichillo, M.G.; Bordoni, M.; Cavalli, M.; Crema, S.; Meisina, C. The role of human activities on sediment connectivity of shallow landslides. *Catena* **2018**, *160*, 261–274. [\[CrossRef\]](#)
70. D’Amato Avanzi, G.; Giannecchini, R.; Puccinelli, A. The influence of the geological and geomorphological settings on shallow landslides. An example in a temperate climate environment: The June 19, 1996 event in northwestern Tuscany (Italy). *Eng. Geol.* **2004**, *73*, 215–228. [\[CrossRef\]](#)
71. Henriques, C.; Zezere, J.S.; Marques, F. The role of the lithological setting on the landslide pattern and distribution. *Eng. Geol.* **2015**, *189*, 17–31. [\[CrossRef\]](#)
72. Eger, A.; Hewitt, A. Soils and their relationship to aspect and vegetation history in the eastern Southern Alps, Canterbury High Country, South Island, New Zealand. *Catena* **2008**, *75*, 297–307. [\[CrossRef\]](#)
73. Dai, F.C.; Lee, C.F.; Li, J.; Xu, Z.W. Assessment of landslide susceptibility on the natural terrain of Lantau Island, Hong Kong. *Environ. Geol.* **2001**, *40*, 381–391.
74. He, Q.; Xu, Z.; Li, S.; Li, R.; Zhang, S.; Wang, N.; Pham, B.T.; Chen, W. Novel entropy and rotation forest-based credal decision tree classifier for landslide susceptibility modeling. *Entropy* **2019**, *21*, 106. [\[CrossRef\]](#) [\[PubMed\]](#)
75. Lee, S.; Min, K. Statistical analysis of landslide susceptibility at Yongin, Korea. *Environ. Geol.* **2001**, *40*, 1095–1113. [\[CrossRef\]](#)
76. Di Crescenzo, G.; Santo, A. Debris slides—Rapid earth flows in the carbonate massifs of the Campania region (Southern Italy): Morphological and morphometric data for evaluating triggering susceptibility. *Geomorphology* **2005**, *66*, 255–276. [\[CrossRef\]](#)
77. Galve, J.P.; Cevasco, A.; Brandolini, P.; Soldati, M. Assessment of shallow landslide risk mitigation measures based on land use planning through probabilistic modelling. *Landslides* **2015**, *12*, 101–114. [\[CrossRef\]](#)
78. Lasanta, T.; Arnáez, J.; Oserín, M.; Ortigosa, L. Marginal Lands and Erosion in Terraced Fields in the Mediterranean Mountains. *Mt. Res. Develop.* **2001**, *21*, 69–76. [\[CrossRef\]](#)
79. Stanchi, S.; Freppaz, M.; Agnelli, A.; Reinsch, T.; Zanini, E. Properties, best management practices and conservation of terraced soils in southern Europe (from Mediterranean areas to the Alps): A review. *Quater. Int.* **2012**, *265*, 90–100. [\[CrossRef\]](#)
80. Tarolli, P.; Preti, F.; Romano, N. Terraced landscapes: From an old best practice to a potential hazard for soil degradation due to land abandonment. *Anthropocene* **2014**, *6*, 10–25. [\[CrossRef\]](#)
81. Brandolini, P.; Cevasco, A.; Capolongo, D.; Pepe, G.; Lovergine, F.; Del Monte, M. Response of terraced slopes to a very intense rainfall event and relationships with land abandonment: A case study from Cinque Terre (Italy). *Land Degrad. Dev.* **2018**, *29*, 630–642. [\[CrossRef\]](#)
82. Cevasco, A.; Pepe, G.; Brandolini, P. The influences of geological and land use settings on shallow landslides triggered by an intense rainfall event in a coastal terraced environment. *Bull. Eng. Geol. Environ.* **2014**, *73*, 859–875. [\[CrossRef\]](#)
83. Agnoletti, M.; Errico, A.; Santoro, A.; Dani, A.; Preti, F. Terraced landscapes and hydrogeological risk. Effects of land abandonment in Cinque Terre (Italy) during severe rainfall events. *Sustainability* **2019**, *11*, 235. [\[CrossRef\]](#)
84. Gökçeoglu, C.; Aksoy, H. Landslide susceptibility mapping of the slopes in the residual soils of the Mengen region (Turkey) by deterministic stability analyses and image processing techniques. *Eng. Geol.* **1996**, *44*, 147–161. [\[CrossRef\]](#)
85. Lucà, F.; Conforti, M.; Robustelli, G. Comparison of GIS-based gully susceptibility mapping using bivariate and multivariate statistics: Northern Calabria, South Italy. *Geomorphology* **2011**, *134*, 297–308. [\[CrossRef\]](#)
86. Guadagno, F.; Martino, S.; Mugnozza, G.S. Influence of man-made cuts on the stability of pyroclastic covers (Campania, southern Italy): A numerical modelling approach. *Environ. Geol.* **2003**, *43*, 371–384. [\[CrossRef\]](#)

87. Tarolli, P.; Calligaro, S.; Cazorzi, F.; Dalla Fontana, G. Recognition of surface flow processes influenced by roads and trails in mountain areas using high-resolution topography. *Eur. J. Remote Sens.* **2013**, *46*, 176–197. [\[CrossRef\]](#)
88. Jaboyedoff, M.; Michoud, M.; Derron, M.-H.; Voumard, J.; Leibundgut, G.; Sudmeier-Rieux, K.; Nadim, F.; Leroi, E. Human-induced landslides: Towards the analysis of anthropogenic changes of the slope environment. In *Landslides and Engineering Slopes—Experiences, Theory and Practices*; Avresa, S., Cascini, L., Picarelli, L., Scavia, C., Eds.; CRC Press: London, UK, 2016; pp. 217–232. [\[CrossRef\]](#)
89. Faccini, F.; Piana, P.; Sacchini, A.; Lazzeri, R.; Paliaga, G.; Luino, F. Assessment of heavy rainfall triggered flash floods and landslides in the Sturla stream basin (Ligurian Apennines, northwestern Italy). *Jokull* **2017**, *67*, 44–73.
90. Giordan, D.; Cignetti, M.; Baldo, M.; Godone, D. Relationship between man-made environment and slope stability: The case of 2014 rainfall events in the terraced landscape of the Liguria region (northwestern Italy). *Geomat. Nat. Haz. Risk* **2017**, *8*, 1833–1852. [\[CrossRef\]](#)
91. Saaty, T.L. A scaling method for priorities in hierarchical structures. *J. Math. Psychol.* **1977**, *15*, 234–281. [\[CrossRef\]](#)
92. Saaty, T.L. *The Analytic Hierarchy Process*; M. Graw-Hill: New York, NY, USA, 1980.
93. Saaty, T.L.; Vargas, L.G. *Models, Methods, Concepts and Applications of the Analytic Hierarchy Process*; Springer Science+Business Media: New York, NY, USA, 2012; p. 175. [\[CrossRef\]](#)
94. Chung, C.J.F.; Fabbri, A.G. Validation of spatial prediction models for landslide hazard mapping. *Nat. Hazards* **2003**, *30*, 451–472. [\[CrossRef\]](#)
95. Carrara, A.; Crosta, G.; Frattini, P. Comparing models of debris-flow susceptibility in the alpine environmental. *Geomorphology* **2008**, *94*, 353–378. [\[CrossRef\]](#)
96. Goepel, K.D. Implementing the Analytic Hierarchy Process as a Standard Method for Multi-Criteria Decision Making. In *Corporate Enterprises—A New AHP Excel Template with Multiple Inputs, Proceedings of the International Symposium on the Analytic Hierarchy Process, Kuala Lumpur, Malaysia, 23–26 June 2013*; Creative Decisions Foundation: Kuala Lumpur, Malaysia, 2013; Volume 2, no. 10; pp. 1–10.
97. Alonso, J.A.; Lamata, M.T. Consistency in the analytic hierarchy process: A new approach. *Int. J. Uncertain. Fuzz.* **2006**, *14*, 445–459. [\[CrossRef\]](#)
98. Saaty, T.L. *Decision Making for Leaders: The Analytical Hierarchy Process. for Decisions in a Complex World*; RWS Publications: Pittsburgh, PA, USA, 2000.
99. Jost, L. Partitioning diversity into independent alpha and beta components. *Ecology* **2007**, *88*, 2427–2439. [\[CrossRef\]](#) [\[PubMed\]](#)
100. Shannon, C. A mathematical theory of communication. *Bell. Syst. Tech. J.* **1948**, *27*, 379–423, 623–656. [\[CrossRef\]](#)
101. Ayalew, L.; Yamagishi, H.; Ugawa, N. Landslide susceptibility mapping using GIS-based weighted linear combination, the case in Tsugawa area of Agano River, Niigata Prefecture, Japan. *Landslides* **2004**, *1*, 73–81. [\[CrossRef\]](#)
102. Pradhan, B.; Youssef, A.M.; Varathrajoo, R. Approaches for delineating landslide hazard areas using different training sites in an advanced artificial neural network model. *Geo-Spat. Inform. Sci.* **2010**, *13*, 93–102.
103. Swets, J.A. Measuring the accuracy of diagnostic systems. *Science* **1988**, *240*, 1285–1293. [\[CrossRef\]](#)
104. Autorità di Bacino Regionale. Piano di Bacino Stralcio per L’assetto Idrogeologico, Ambito 15 [Basin Master Plan for the Geo-Hydrological Arrangement]. Available online: <http://www.pianidibacino.ambienteinliguria.it/GE/ambito15/ambito15.html> (accessed on 15 December 2020).
105. van Vliet, J.; Bregt, A.K.; Hagen-Zanker, A. Revisiting Kappa to account for change in the accuracy assessment of land-use change models. *Ecol. Model.* **2011**, *222*, 1367–1375. [\[CrossRef\]](#)
106. Baeza, C.; Lantada, N.; Amorim, S. Statistical and spatial analysis of landslide susceptibility maps with different classification systems. *Environ. Earth Sci.* **2016**, *75*, 1318. [\[CrossRef\]](#)
107. Visser, H.; de Nijs, T. The Map Comparison Kit. *Environ. Model. Softw.* **2006**, *21*, 346–358. [\[CrossRef\]](#)
108. Lateltin, O.; Haemmig, C.; Raetzo, H.; Bonnard, C. Landslide risk management in Switzerland. *Landslides* **2005**, *2*, 313–320. [\[CrossRef\]](#)
109. Li, G.; Lei, Y.; Yao, H.; Wu, S.; Ge, J. The influence of land urbanization on landslides: An empirical estimation based on Chinese provincial panel data. *Sci. Total Environ.* **2017**, *595*, 681–690. [\[CrossRef\]](#) [\[PubMed\]](#)
110. Turconi, L.; Faccini, F.; Marchese, A.; Paliaga, G.; Casazza, M.; Vojinovic, Z.; Luino, F. Implementation of nature-based solutions for hydro-meteorological risk reduction in small Mediterranean catchments: The case of Portofino Natural Regional Park. *Sustainability* **2019**, *12*, 1240. [\[CrossRef\]](#)